Article

Current Biology

Ovulation suppression protects against chromosomal abnormalities in mouse eggs at advanced maternal age

Graphical abstract

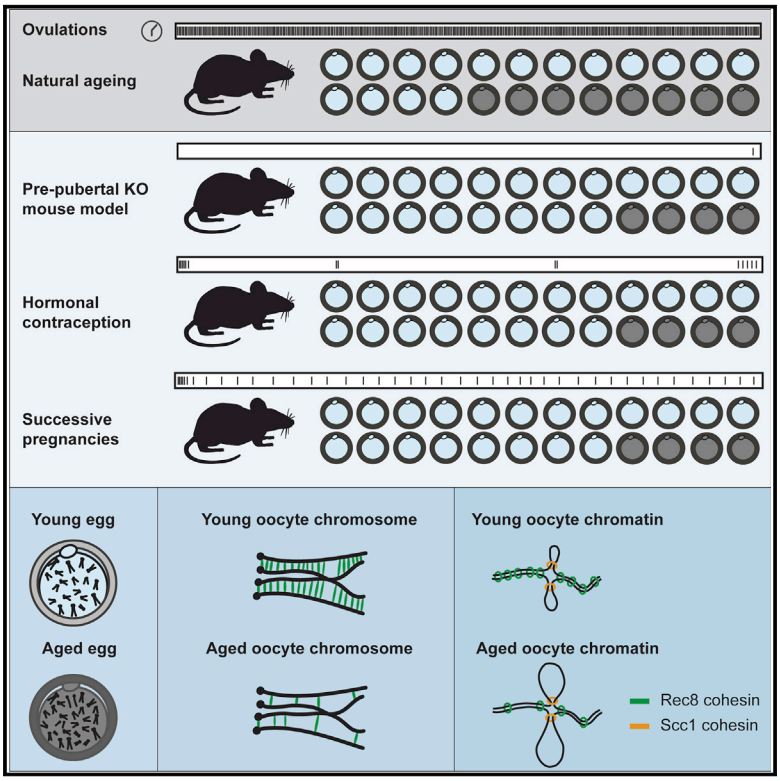

Highlights

- Ovulation reduction protects against Rec8 loss and egg aneuploidy in aged female mice
- Ovulations contribute to physiological aging of oocytes and the maternal age effect
- Cellular aging is associated with changes in 3D chromatin organization
- Cohesin complexes mediating sister chromatid cohesion restrict loop extrusion

Authors

Emmanouella E. Chatzidaki, Sean Powell, Bart J.H. Dequeker, Johanna Gassler, Mariana C.C. Silva, Kikuë Tachibana

Correspondence

tachibana@biochem.mpg.de

In brief

Chatzidaki et al. discover that the physiological aging of oocytes can be delayed by reducing ovulations: studies in three mouse models converge on showing that ovulations contribute to meiosis I chromosome segregation errors and chromosomal abnormalities in eggs of aged female mice.

Chatzidaki et al., 2021, Current Biology *31*, 4038–4051
September 27, 2021
https://doi.org/10.1016/j.cub.2021.06.076

CellPress

CellPress
OPEN ACCESS

Current Biology

Article

Ovulation suppression protects against chromosomal abnormalities in mouse eggs at advanced maternal age

Emmanouella E. Chatzidaki,[1] Sean Powell,[1,4] Bart J.H. Dequeker,[1,4] Johanna Gassler,[1] Mariana C.C. Silva,[2] and Kikuë Tachibana[1,3,5,*]

[1]Institute of Molecular Biotechnology of the Austrian Academy of Sciences, Vienna BioCenter, Dr. Bohr-Gasse 3, 1030 Vienna, Austria
[2]Research Institute of Molecular Pathology, Campus Vienna BioCenter 1, 1030 Vienna, Austria
[3]Department of Totipotency, Max Planck Institute of Biochemistry, Am Klopferspitz 18, 82152 Martinsried, Munich, Germany
[4]These authors contributed equally
[5]Lead contact
*Correspondence: tachibana@biochem.mpg.de
https://doi.org/10.1016/j.cub.2021.06.076

SUMMARY

The frequency of egg aneuploidy and trisomic pregnancies increases with maternal age. To what extent individual approaches can delay the "maternal age effect" is unclear because multiple causes contribute to chromosomal abnormalities in mammalian eggs. We propose that ovulation frequency determines the physiological aging of oocytes, a key aspect of which is the ability to accurately segregate chromosomes and produce euploid eggs. To test this hypothesis, ovulations were reduced using successive pregnancies, hormonal contraception, and a pre-pubertal knockout mouse model, and the effects on chromosome segregation and egg ploidy were examined. We show that each intervention reduces chromosomal abnormalities in eggs of aged mice, suggesting that ovulation reduction delays oocyte aging. The protective effect can be partly explained by retention of chromosomal Rec8-cohesin that maintains sister chromatid cohesion in meiosis. In addition, single-nucleus Hi-C (snHi-C) revealed deterioration in the 3D chromatin structure including an increase in extruded loop sizes in long-lived oocytes. Artificial cleavage of Rec8 is sufficient to increase extruded loop sizes, suggesting that cohesin complexes maintaining cohesion restrict loop extrusion. These findings suggest that ovulation suppression protects against Rec8 loss, thereby maintaining both sister chromatid cohesion and 3D chromatin structure and promoting production of euploid eggs. We conclude that the maternal age effect can be delayed in mice. An implication of this work is that long-term ovulation-suppressing conditions can potentially reduce the risk of aneuploid pregnancies at advanced maternal age.

INTRODUCTION

The maternal age effect is the socio-pathological phenomenon that the frequency of trisomic pregnancies increases dramatically with maternal age. The incidence of trisomic pregnancies is 3% for women in their 20s and rises to >30% for women in their 40s.[1] The incidence differs between chromosomes, for example, chromosome 16 trisomy increases linearly with age whereas chromosome 21 trisomy (Down syndrome) increases exponentially in the mid-30s. Most trisomies arise from chromosome missegregation in the meiosis I division of female germ cells (oocytes).[2–5] The resulting aneuploid eggs produce aneuploid fetuses upon fertilization. Aneuploidy is the leading cause of mental retardation and miscarriages.[6] Most aneuploid pregnancies with the exception of trisomy 21, trisomy 18 (Edward syndrome), trisomy 13 (Pätau syndrome), and monosomy X0 (Turner syndrome) are incompatible with life.[7] Despite understanding the etiology of trisomic pregnancies, the causes of increased chromosome missegregation in aging oocytes have remained enigmatic.

The biology of oocytes may provide insights into the causes of increased egg aneuploidy with maternal age.[7–9] Mammalian oocytes are generated during fetal development. After birth, oocytes remain arrested for months in the mouse and decades in the human until, periodically, some grow into mature oocytes in sexually mature females. Ovulation triggers the first meiotic division that produces eggs, which remain arrested until fertilization. To place chromosome biology into the context of oogenesis, meiotic DNA replication occurs in fetal oocytes. At this stage, sister chromatid cohesion mediated by Rec8-cohesin complexes (hereafter referred to as Rec8) is established and cannot be regenerated thereafter.[10,11] Fetal oocytes undergo meiotic recombination, where reciprocal crossovers of maternal and paternal homologous chromosomes result in the formation of meiosis-specific chromosome structures termed bivalents. Fully grown mature oocytes undergo germinal vesicle breakdown (GVBD), and bivalent chromosomes align on the spindle with maternal and paternal centromeres oriented toward opposite spindle poles (bi-orientation) during the meiosis I division. Cleavage of Rec8 along chromosome arms releases arm

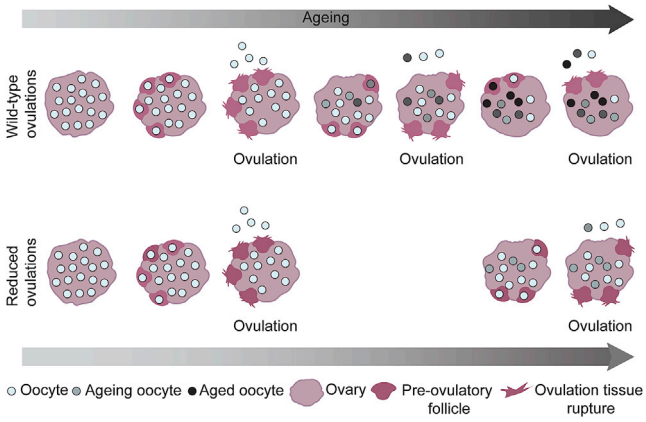

Figure 1. Model for the incessant ovulation hypothesis

Oogonia are arrested in the dictyate stage of late prophase of the first meiotic division in the developing follicles of the ovary. A small proportion of these follicles will reach the ovulatory stage whereas most will be lost to apoptosis. Every ovulation occurs by rupture of the ovarian epithelial layer via a wound-generating process, damaging nearby resting oocytes in the ovarian stroma. Within oocytes, long-lived molecules including DNA and proteins, which are not turned over, such as Rec8-cohesin are particularly prone to repeated damage. As ovulations continue, damage accumulates, as depicted by darker colored oocytes, some of which will be ovulated at a later stage. Reduced ovulations (indicated by the dashed arrow) limit ovulation-induced damage and promote retention of oocyte health.

cohesion, and maternal and paternal centromeres segregate during anaphase I into the egg and the first polar body (PB). In meiosis II, dyad chromosomes consisting of sister chromatids that have undergone recombination align at the metaphase plate of eggs. Fertilization triggers the completion of the meiosis II division. Cleavage of centromeric Rec8 releases sister centromere cohesion, and individual chromatids segregate during anaphase II into the egg or the second PB.

Several hypotheses have been proposed to explain the increased frequency of chromosome missegregation in oocytes at advanced maternal age. The frequency and placement of crossovers as well as defective crossover maturation during meiotic recombination in fetal oocytes can predispose toward chromosome missegregation.[12–14] The fidelity of chromosome segregation is also compromised by error-prone spindle assembly and a weak spindle assembly checkpoint.[15–21] These provide explanations for the higher frequency of aneuploidy in eggs compared to other cell types but cannot alone explain the increase in aneuploidy with maternal age, which requires that another variable changes with time. One hypothesis is that the decrease in oocyte pool with age affects the quality of remaining oocytes.[22,23] However, human data show no correlation between oocyte pool size and aneuploidy.[24–26]

Another hypothesis is that the irreversible loss of Rec8-containing cohesin leads to weakening or loss of cohesion, chromosome missegregation, and aneuploidy.[27] This is supported by evidence from aged mice, where chromosomal Rec8 decreases to below threshold detection.[28,29] Both mouse and human oocytes show evidence of cohesion weakening at sister centromeres and chromosome arms with age.[11,27–30] It is thought that loss of arm cohesion can be responsible for homolog nondisjunction and egg aneuploidy. Weakening of sister centromere cohesion can result in aberrant sister kinetochore bi-orientation,[20] precocious loss of sister centromere cohesion (PSCC), random segregation of chromatids in eggs, and potential fetal aneuploidy.[11,27–30] In addition to cell-intrinsic mechanisms, exposure to environmental toxins like bisphenol A (BPA) and oxidative damage by reactive oxygen species (ROS) can cause aneuploid pregnancies.[31–33]

The maternal age effect occurs over decades in humans and over months in mice and is therefore thought to reflect the physiological, rather than chronological, aging of oocytes.[6] Here, we test whether the physiological aging of oocytes can be delayed by reducing ovulations. Using three mouse models that converge on reducing ovulations, we show that each displays fewer chromosomal abnormalities in eggs of aged females compared to control aged females. The rescue in abnormalities correlates with retention of chromosomal Rec8-cohesin, suggesting that ovulations contribute to cohesin deterioration. Unexpectedly, Rec8 loss also affects loop extrusion and may contribute to the 3D chromatin changes observed in long-lived oocytes. Our findings reveal that ovulation suppression protects against chromosomal abnormalities in eggs at advanced maternal age.

RESULTS

Hypothesis that ovulation frequency determines the physiological aging of oocytes

To gain insights into the physiological aging of oocytes, we considered the cells in the context of the ovarian tissue. Ovaries harbor all oocytes that will determine the reproductive lifespan of a female. Oocytes are ovulated every 28 days in humans and every 4 days in mice, with the latter ovulating several oocytes at once. Ovulations rupture the epithelial tissue,[34] akin to a wound, releasing ROS that damage nucleic acids and proteins in neighboring cells. Indeed, oxidative base (8-oxoguanine) damage has been detected in epithelial cells near sites of ovulations in sheep ovaries.[35] Oocytes residing in the ovary that have not been ovulated are therefore expected to be exposed to repeated cycles of ROS, released after every ovulation. Increased oxidative stress (e.g., as induced by a high fat diet) is linked to egg aneuploidy.[36–38] More directly, increased ROS in *Drosophila* oocytes causes cohesion weakening and homolog non-disjunction.[33] Together, we propose that ovulations, by damaging resting oocytes, determine the physiological aging of mammalian oocytes (Figure 1).

Successive pregnancies reduce chromosomal abnormalities in eggs of aged females

A prediction of the hypothesis is that preventing the repetitive injury and repair process of ovulations should limit the increase in chromosome segregation errors and chromosomal abnormalities in eggs with age (Figure 1). We therefore tested the effects of successive pregnancies on meiosis I chromosome segregation in oocytes isolated from 14- to 15-month-old animals. Males and females were maintained in a cage to promote post-partum mating, which naturally reduces ovulation frequency from every 4 to every 21 days (Figure S1A), and control virgin females were maintained with male bedding to promote estrus cycling. Although the number of ovulations that occurred in virgin females cannot be determined, females in constant mating underwent

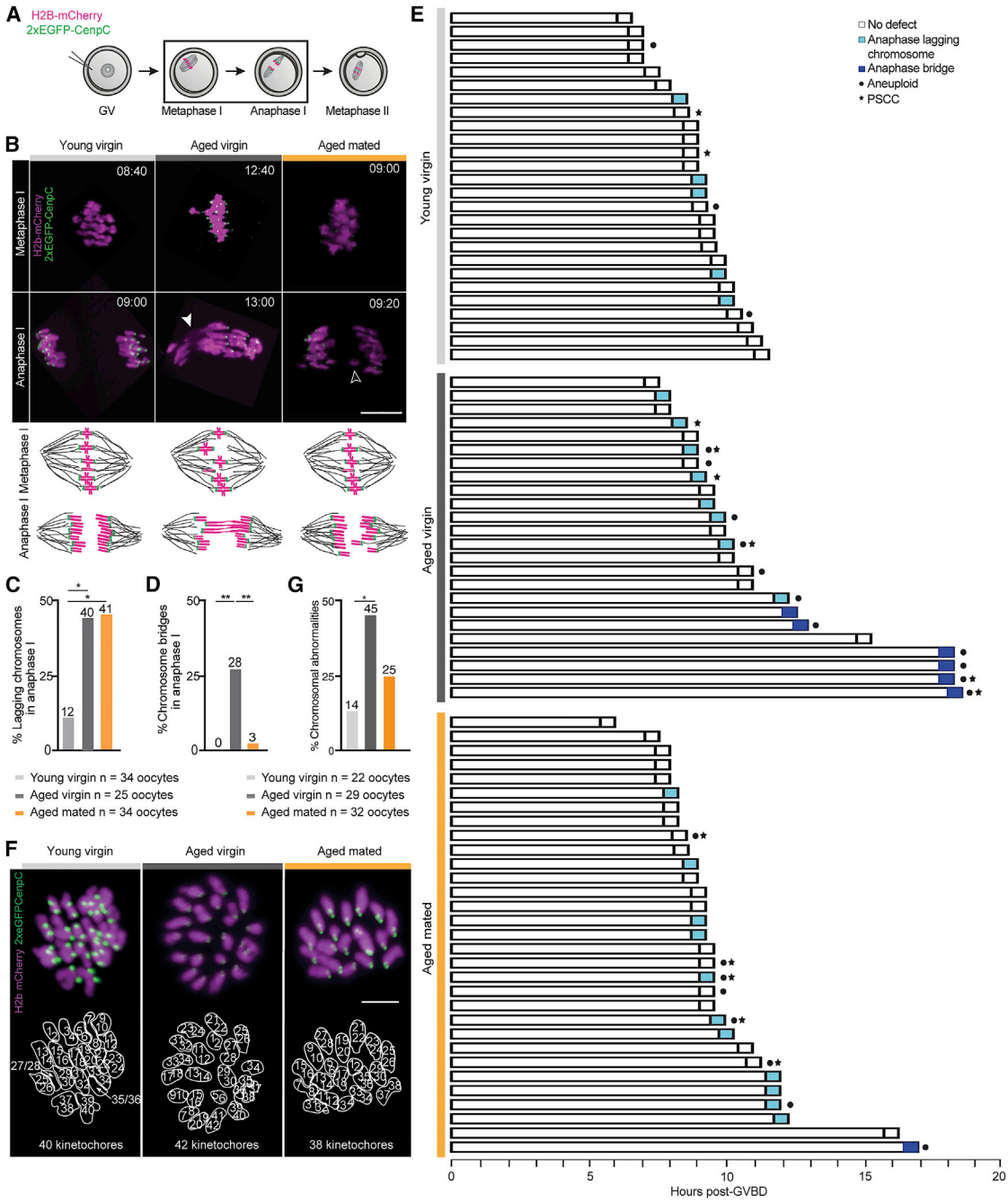

Figure 2. Naturally reducing ovulations by pregnancy reduces the incidence of anaphase bridges and chromosomal abnormalities in *in situ* fixed metaphase II eggs

(A) Mature GV oocytes were injected with H2B-mcherry and 2xEGFP-CenpC mRNA to mark chromosomes and kinetochores during meiosis I division.

(B) Representative time-lapse frames from high-resolution live-cell imaging of the meiosis I division, tracking DNA (magenta) and kinetochores (green). Images represent metaphase (single time point before anaphase) and anaphase (time stamps h:min from GVBD). Empty arrow head indicates a lagging chromosome (anaphase). Filled arrow head indicates anaphase bridges. Schematic representation of metaphase and anaphase state for each condition.

(C) Time-lapse microscopy reveals that the age-dependent increase in anaphase I chromosome misalignment (lagging chromosomes) is unaffected by reducing ovulation number (young versus aged virgin $p = 0.02$; young versus aged mated $p = 0.01$).

(D) Time-lapse microscopy reveals that the age-dependent increase in the incidence of anaphase I bridges is significantly reduced in aged mated females (young versus aged virgin $p = 0.001$; aged virgin versus aged mated $p = 0.008$).

(E) Longitudinal time course plots of all oocytes where anaphase I and ploidy status in metaphase II could be determined. Oocyte numbers from: young virgin = 26; aged virgin = 24; aged mated = 31. Clear bar represents the time till metaphase. Clear square represents no metaphase or anaphase error. Light blue square

(legend continued on next page)

fewer ovulations because each had an average of 5 to 6 litters. Another limitation inherent to oocyte/egg studies is that only a proportion of oocytes in the ovary is fully grown at any time point and can therefore be examined for chromosome segregation. We therefore assume, but cannot know for certain, that the results obtained in the proportion of examined oocytes are representative of all oocytes in the ovary.

To examine how successive pregnancies affected the meiosis I division of oocytes, we followed chromosome dynamics by 4D live-cell imaging. Germinal vesicle (GV)-stage oocytes were microinjected with mRNA encoding H2B-mCherry to mark chromosomes and CenpC-EGFP to mark kinetochores. Following GVBD, chromosomes were tracked during the meiosis I division until metaphase II (Figures 2A–2E and S1H; Videos S1, S2, S3, S4, and S5). We quantified chromosome segregation errors in anaphase I into: (1) lagging chromosomes, in which individual chromosomes are closer to the spindle midzone than the mass of anaphase chromosomes, and (2) chromosome bridges, in which a continuous mass of DNA spans the spindle midzone and kinetochore signals are oriented toward each pole. Lagging chromosomes increased from 12% to 40% with age in oocytes from virgin females, and to 41% in aged mated females ($p < 0.01$) (Figure 2C), suggesting that ovulation reduction has no effect on the frequency of lagging chromosomes. On the other hand, chromosome bridges were rarely observed in oocytes from young virgin females and increased to 28% in oocytes from aged virgin females ($p = 0.001$) (Figure 2D) and only to 3% in oocytes from aged mated females ($p > 0.9$) (Figure 2D), suggesting that ovulation reduction protects against chromosome bridge formation.

To examine the consequences of segregation errors on the chromosomal content of eggs, 3D reconstructions of metaphase II chromosomes were performed after live-cell imaging for each cell. Euploid mouse eggs contain 20 pairs of sister chromatids (dyad chromosomes) and 20 pairs of sister kinetochores. Single kinetochores indicate precocious loss of sister centromere cohesion (PSCC), which will lead to random segregation during the meiosis II division (Figure S1B). Together, we quantified as ''chromosomal abnormalities'' (Figure 2G) the cells that include both altered numbers of sister kinetochores (''chromosomal aneuploidy'') and PSCC (Figures S1J–S1L). Chromosomal abnormalities increased from 14% in eggs from young virgin to 45% in eggs from aged virgin females ($p = 0.03$) and to 25% in eggs from aged mated females ($p = 0.5$); subsequent experiments with larger cell numbers resulted in a statistically significant difference in chromosomal abnormalities between eggs from aged virgin and aged mated females (Figures 3D, S1C, and S1E). Unexpectedly, lagging chromosomes led to chromosomal abnormalities in only 47% of eggs (9/19 cells) (Figure 2E), suggesting that many lagging chromosomes eventually segregate properly and are captured on the meiosis II spindle; this is unlike in mitotically proliferating cells, where lagging chromosomes can form micronuclei.[39] Chromosome bridges resulted in chromosomal abnormalities in 6/7 cells, suggesting that these have a more detrimental effect (Figure 2E). Because the chromosome bridges were observed in oocytes from aged females, they were presumably not generated by meiotic recombination but through mechanisms occurring during aging. Further experiments are needed to ascertain these findings.

To exclude that live-cell imaging exacerbated chromosome segregation errors, we also analyzed chromosome spreads of metaphase II eggs that had not been imaged live (Figures 3 and S1C–S1G). Aneuploidy data for hyper- and hypoploidy was scored separately due to potential chromosome loss as a technical artifact but no significant differences were found (Figures S1C–S1G). Chromosomal aneuploidy (hyper- and hypoploidy) was detected in 6% of eggs from young virgin females. Chromosomal aneuploidy increased to 28% and 15% of eggs from aged virgin and mated females, respectively (Figure S1F) ($p = 0.12$). Total chromosomal abnormalities in eggs increased from 7% in young virgin female eggs to 37% in eggs from aged virgin females ($p = 0.0014$), but only to 17% from aged mated females (Figure 3D) ($p = 0.04$). Therefore, ovulation reduction resulted in an ~2-fold decrease in chromosomal abnormalities. This suggests that interrupting incessant ovulations with pregnancies offers some degree of protection against the age-related increase in chromosomal abnormalities.

A key question is how ovulations affect the proteins required for chromosome segregation. Rec8 decreases on chromosomes with age ($p < 0.001$) (Figures S2A–S2C), as reported previously.[28] We hypothesized that Rec8 damage induced by ovulations leads to its deterioration. If so, then Rec8 should be more abundant on chromosomes in oocytes from aged mated than aged virgin females. To test this, we examined chromosomal Rec8 abundance in *in situ* fixed oocytes (Figures 4A–4C). Chromosomal Rec8 was nearly undetectable in oocytes from aged virgin females and more abundant on chromosomes and centromeres in oocytes from aged mated females ($p < 0.0001$) (Figures 4A–4C). Since Rec8 is essential for sister kinetochore mono-orientation in meiosis I and sister centromere cohesion in meiosis II, Rec8 retention is a plausible explanation for the rescue of PSCC following ovulation reduction (Figures S1D, S1G, S1K, S3C, and S4J). We conclude that successive pregnancies protect against Rec8 loss from chromosomes and suggest that this is due to reduced ovulation frequency.

marks the presence of lagging chromosome at anaphase. Dark blue square marks the presence of anaphase bridges. Dot represents incorrect kinetochore number and star, the presence of PSCC.

(F) Representative images of 3D reconstruction from the metaphase II plate of eggs, following live cell imaging, paired with arithmetical representation of present kinetochores from young virgin, aged virgin, and aged mated females. The chromosome area is marked by a line, that encircles the numbered kinetochores. Images generated with Fiji software.

(G) 3D reconstruction of the metaphase II plate after live cell imaging. Incidence of chromosomal abnormalities increases with age but half as much when reducing ovulations with constant mating (young versus aged virgin $p = 0.03$; aged virgin versus aged mated $p = 0.1$). Chromosomal abnormalities include any anomaly from 20 intact dyad chromosomes (PSCC and chromosomal aneuploidy).

Number of females used: young virgin = 16; aged virgin = 31; aged mated = 18. n value represents the number of oocytes included. Statistical analysis for meiosis I observations was done using a two-sided Fisher's exact test. Scale bar, 10 μm. *$p < 0.05$ **$p < 0.01$, ***$p < 0.001$. See also Figure S1 and Videos S1, S2, S3, S4, and S5.

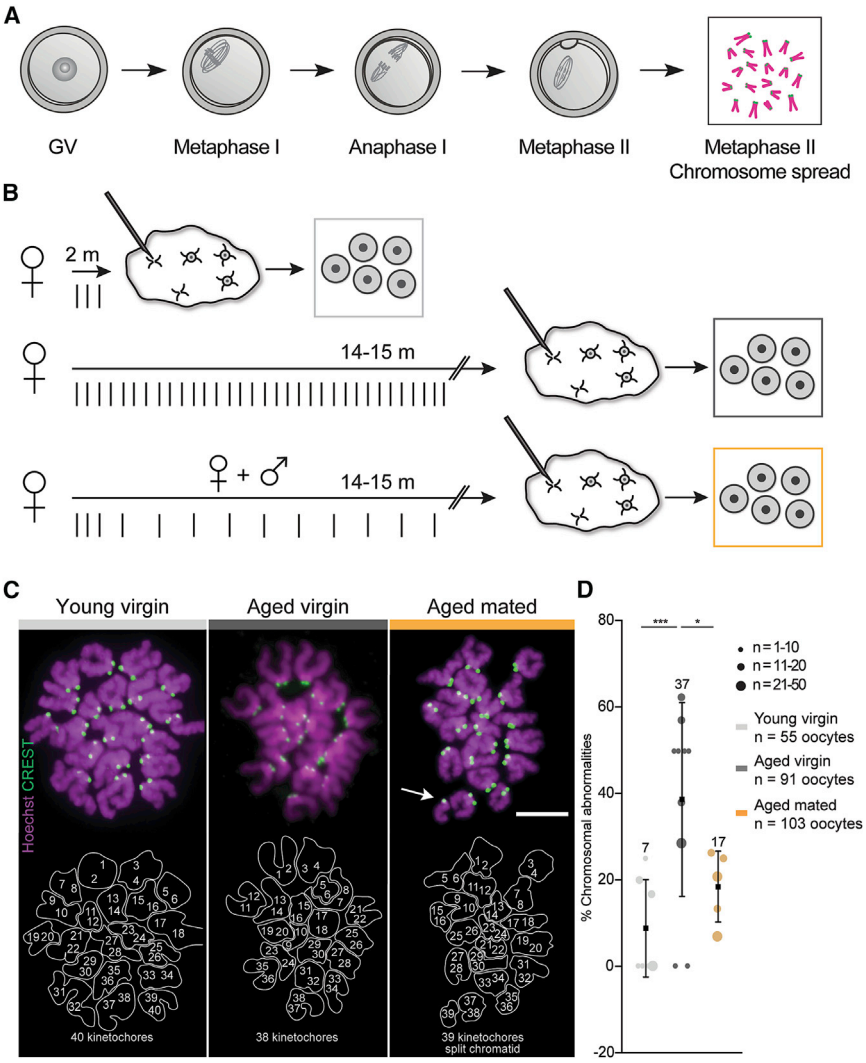

Figure 3. Naturally reducing ovulations by pregnancy significantly reduces the incidence of chromosomal abnormalities in chromosome spreads

(A) Mature GV oocytes underwent the meiosis I division *in vitro* and were collected in meiosis II for chromosome spreading.

(B) Oocyte retrieval from ovaries of young (few ovulations, light gray), aged virgin (many ovulations, dark gray), and aged females mated from 2 months (reduced ovulations, orange). Vertical lines represent ovulations.

(C) Representative images of MII chromosome spreads with arithmetical representation of kinetochores from young virgin, aged virgin, and aged females in constant mating. Arrow indicates a separated sister chromatid. The chromosome area is marked by a line that encircles the numbered kinetochores. Scale bar, 10 μm.

(D) Incidence of chromosomal abnormalities from metaphase II chromosome spreads. Individual circles represent separate experiments; the sizes vary according to the sample size of each experiment. Cubes represent the weighted mean of each condition with weighted SD error bars (young versus aged virgin $p = 0.00015$; aged virgin versus aged mated $p = 0.005$; young versus aged mated $p = 0.013$). Chromosomal abnormalities include any anomaly from 20 intact dyad chromosomes (PSCC and chromosomal aneuploidy). Number of females used: young virgin = 12; aged virgin = 53; aged mated = 23. n value represents the number of oocytes included unless otherwise stated. Statistical analysis for metaphase II ploidy was done using a weighted two-tailed paired Welch t test. *$p < 0.05$ **$p < 0.01$, ***$p < 0.001$.

See also Figure S1.

3D chromatin organization deteriorates in long-lived oocytes

We also considered whether ovulations affect other aspects of chromosome biology. Whether 3D chromatin structure changes during natural aging is not known. We asked whether there are detectable changes and, if so, whether these depend on ovulations. Single-nucleus Hi-C (snHi-C) detects genome-wide proximity contacts and can be used to investigate chromatin loops, which are hypothesized to be generated by a mechanism of loop extrusion.[40,41] Stalling of loop extrusion at CTCF bound to its cognate motif results in anchored loops.[42] These are detected in snHi-C data by averaging over loop coordinates that were called *de novo* in mouse embryonic fibroblasts[43] (Figure 4D). Extruded loops result in variable contacts and are inferred from contact probability plots (Figure 4D). snHi-C was performed on GV-stage oocytes because the protocol requires a nucleus for manipulation. Little differences were observed in aggregate loop strengths for oocytes from young versus aged C57BL/6 females (Figures 4E and S2D; Table S1).

To investigate extruded loops, we examined contact probabilities over increasing genomic distance. Unexpectedly, contacts decreased over the range of up to 5 Mb in oocytes from aged compared to young females (Figures S2G and S2I). The first maximum of the scaling plot derivative provides an estimated size of an average extruded loop[44] (Figures 4D, 4F, and S2E). Bootstrapping of all slopes of the corresponding young and aged curves was performed, and the slope averages were plotted for statistical testing. Interestingly, average loop sizes increase from 310 kbp to 420 kbp with age (Figures 4F and 4G) ($p = 10^{-18}$), which appears to vary according to strain background and does not strongly depend on ovulations (Figures S2E–S2J). Larger average loop sizes imply that loop extrusion can proceed for longer (processivity) and suggests that a barrier deteriorates with age. Presumably the barrier is not predominantly CTCF, otherwise aggregate loop strength would be expected to decrease to a greater extent.[45] Together, these results provide the first evidence that 3D chromatin organization deteriorates in oocytes and raise the possibility that the phenomenon might occur in other long-lived cells.

We further considered what might constitute the potential loop extrusion impediment that deteriorates with age. Loop extrusion depends on Scc1-containing cohesin complexes and sister chromatid cohesion is mediated by Rec8-containing cohesin complexes in oocytes.[43,46] Whether extruding cohesin can

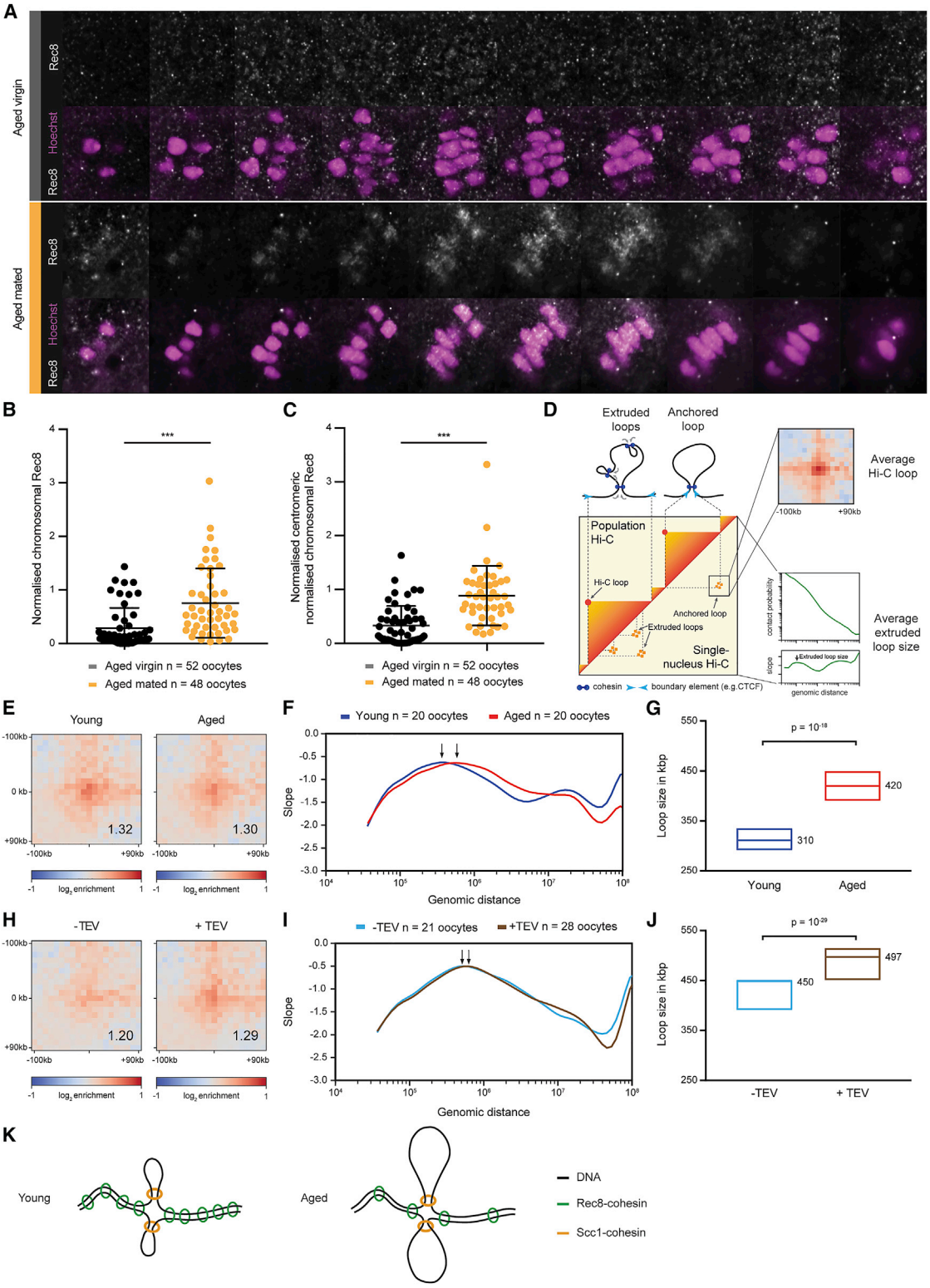

Figure 4. Reducing ovulations by pregnancy allows for significantly increased retention of Rec8 cohesin and for retention of extruded loops suggesting cohesive cohesin is a barrier for loop extrusion

(A) Representative images of acquired metaphase I *Z* stacks from *in situ* fixed oocytes of aged virgin and mated C57BL/Icrf^{at} females. Six to eight slices from each *Z* stack were collapsed (sum of slices) to generate the respective images in the series. Scale bar, 5 μm.

(legend continued on next page)

bypass a cohesin complex mediating cohesion is unclear. Cohesive Rec8-cohesin might pose an obstacle to extruding Scc1-cohesin, and Rec8 loss would lead to an increase in extruded loop sizes. Alternatively, other proteins degrade with age and affect chromatin loops. To distinguish between these possibilities, we performed a sufficiency experiment in young oocytes, in which Scc1 release from chromosomes is prevented due to lack of the cohesin release factor Wapl, and Rec8 is engineered to contain TEV protease recognition sites[11,43,44,46–48] (Figures 4H–4J, S2K, and S2L; Table S1). *Rec8*$^{TEV/TEV}$ *Wapl*$^{\Delta/\Delta}$ oocytes were isolated from *Rec8*$^{TEV/TEV}$ *Wapl*$^{fl/fl}$ *(Tg)Zp3*-Cre females, microinjected with mRNA encoding TEV protease, and snHi-C was performed. Average loop strength increased after TEV protease expression to cleave Rec8, which is consistent with loop extrusion proceeding to CTCF anchors after removal of a barrier (Figure 4H) ($p = 0.00049$; see STAR Methods). Average loop sizes in *Rec8*$^{TEV/TEV}$*Wapl*$^{\Delta/\Delta}$ oocytes without TEV protease expression are larger than in wild-type oocytes, which is due to the increase in Scc1 residence time on chromosomes and extended loop extrusion. Importantly, expression of TEV protease to cleave Rec8, caused an increase in average loop sizes from 450 kbp to 515 kbp (515 kbp; Figures 4I, 4J, S2K, and S2L) ($p = 10^{-29}$), demonstrating that Rec8 loss is sufficient to increase average loop sizes. This finding suggests that Rec8 loss can partly explain the increase in average loop size with age, but current data do not allow us to exclude that other barriers also degrade (Figure 4K). We conclude that cohesive cohesin preserves 3D chromatin structure in addition to being essential for chromosome segregation and production of euploid eggs.

Hormonal contraception reduces chromosomal abnormalities in eggs of aged females

Although the rescue in chromosomal abnormalities observed in the successive pregnancies model is consistent with the ovulation hypothesis, this approach cannot distinguish whether the protective effect is due to ovulation reduction or any pregnancy-associated change. We therefore considered it important to further test the hypothesis using other models, each with their own limitations, but converging on the common denominator of reducing ovulations. Oral contraceptive delivery in mice improved litter production,[49] consistent with the possibility that ovulations contribute to the age-related decline in fertility. However, the mechanism underlying this phenomenon and the effects on egg ploidy remain unclear.

Hormonal contraception prevents pregnancies by preventing ovulations and implantation. To investigate whether prolonged hormonal contraception limits the age-dependent egg aneuploidy increase, placebo or medroxyprogesterone slow-releasing (90-day) pellets were implanted into 2-month-old females. The procedure was repeated at 5 and 8 months and the mice were aged until 14 months (Figures 5A and 5B). Female fertility was not affected by the placebo pellet, whereas progesterone-releasing pellets rendered females infertile, which were assessed by the absence of pregnancies during the pellet activity period, implying that ovulations were suppressed. Although it would be ideal to examine all aspects of the meiosis I to II transition, as carried out above, experiments in the additional mouse models focused on chromosomal abnormalities as the most important assay for oocyte aging.

To assess chromosomal abnormalities, we performed *in situ* fixation of eggs to capture all chromosomes and avoid technical caveats associated with chromosome spreads. Chromosomal abnormalities were detected in 36% of eggs from placebo-treated aged females and in only 15% of eggs from progesterone-treated aged females ($p = 0.05$) (Figures 5C, 5D, and S3). The >2-fold reduction in chromosomal abnormalities in mice treated with hormonal contraceptives provides additional support that ovulations contribute to oocyte aging. A key implication

(B) Immunofluorescent staining of oocytes was performed using antibodies against Rec8 (gray) and DNA was stained with Hoechst (magenta). Rec8 chromosomal intensity normalized against background ($p < 0.0001$; non parametric Mann Whitney U statistical test). Data pooled from three independent experiments.

(C) Centromeric Rec8 chromosomal intensity normalized against background ($p < 0.0001$; non parametric Mann Whitney U statistical test). Data pooled from three independent experiments. *$p < 0.05$ **$p < 0.01$, ***$p < 0.001$.

(D) Schematic representation of anchored loops and extruded loops as seen in single-nucleus Hi-C data compared to bulk Hi-C. Anchored loops are stalled at boundary elements and detected upon averaging over loop coordinates detected in MEFs. Extruded loops result in variable contacts in both bulk Hi-C and snHi-C maps. The average extruded loop size can be inferred from the maximum slope of $\log(P_c(s))$ curves.

(E) The strength of average loops between C57BL/6J young (2 months; n = 20) and aged (14–18 months; n = 20). For the average loop strength calculation for each condition (young = 1.32; aged = 1.30) see STAR Methods. The heatmaps were normalized to an equal number of reads.

(F) Slope of the average $\log(P_c(s))$ curve for C57BL/6J young (blue) and aged (red) conditions (see Figure S2G for $P_c(s)$ curves). Arrows indicate the maximum slope, which is used to infer the average size of the extruded loops.

(G) Boxplots of all average loop sizes between C57BL/6J young (2 months, blue) and aged (14–18 months, red) show a significant difference (n(young) = 20 and n(aged) = 20) ($p = 10^{-18}$). Our analysis showed average loop size to be 310 kbp and 420 kbp, respectively. The average loop size per condition is determined by bootstrapping 100 times over the samples within the condition.

(H) The strength of average loops between securin-EGFP mRNA- (−TEV, cyan) injected and TEV protease- and securin-EGFP mRNA- (+TEV, brown) injected *Rec8*$^{TEV/TEV}$ *Wapl*$^{\Delta/\Delta}$ GV oocytes (n(−TEV) = 21 and n(+TEV protease) = 28). For the average loop strength calculation for each condition (−TEV = 1.20; +TEV = 1.29) see STAR Methods. The heatmaps were normalized to an equal number of reads.

(I) Slope of the average $\log(P_c(s))$ curve for −TEV (cyan) and +TEV (brown) protease injected *Rec8*$^{TEV/TEV}$ *Wapl*$^{\Delta/\Delta}$ oocytes (see Figure S2I for $P_c(s)$ curves). Arrows indicate the maximum slope, which is used to infer the average size of the extruded loops.

(J) Boxplots of all average loop sizes between securin-EGFP mRNA injected (−TEV, cyan) and TEV protease- and securin-EGFP mRNA injected (+TEV, brown) *Rec8*$^{TEV/TEV}$ *Wapl*$^{\Delta/\Delta}$ GV oocytes (n(−TEV) = 21 and n(+TEV) = 28) ($p = 10^{-29}$). Our analysis showed this to be 450 kbp and 497 kbp, respectively. The average loop size per condition is determined by bootstrapping 100 times over the samples within the condition.

(K) Model depicting how Rec8 loss can partly explain the increase in average loop size with age.

The p values were determined using the Wilcoxon signed-rank test unless otherwise stated. See also Figure S2 and Table S1.

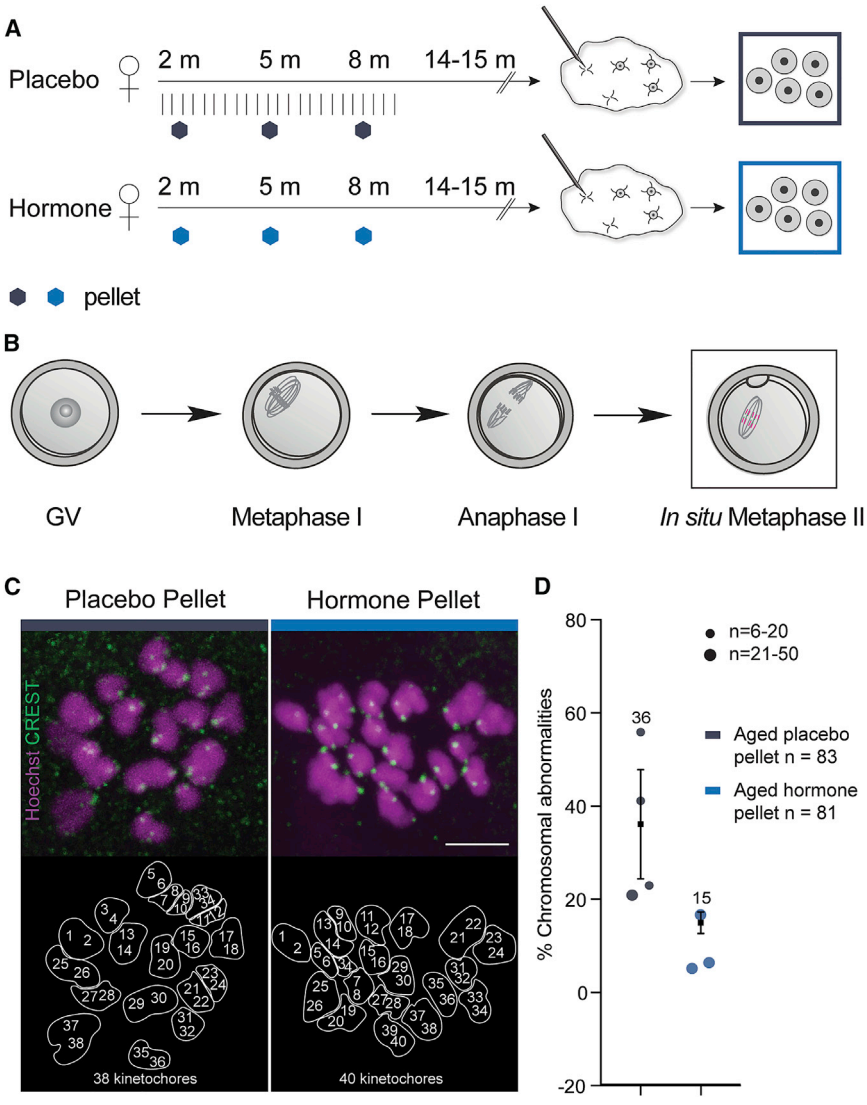

Figure 5. Reducing ovulations by hormonal contraception reduces the incidence of chromosomal abnormalities in MII eggs of aged females

(A) Oocyte retrieval from ovaries of virgin aged C57BL/Icrf^{at} mice implanted with placebo or hormone (progesterone) slow release pellet at 2, 5, and 8 months of age. Vertical lines represent ovulations.

(B) Mature GV oocytes completed meiosis I *in vitro* and were fixed in meiosis II for immunofluorescent staining of kinetochores.

(C) Representative images of 3D reconstruction from the metaphase II plate of eggs paired with arithmetical representations of kinetochores. DNA is stained with Hoechst dye and kinetochore proteins are detected with CREST antibody. Images generated with Fiji software. The chromosome area is marked by a line that encircles the numbered kinetochores. Scale bar, 10 μm.

(D) Incidence of chromosomal abnormalities in MII eggs from aged placebo or hormone-implanted aged C57BL/Icrf^{at} mice ($p = 0.05$). Individual circles represent separate experiments; the sizes vary according to the sample size of each experiment. Cubes represent the weighted mean of each condition with weighted SD error bars. Chromosomal abnormalities include any anomaly from 20 intact dyad chromosomes. Number of females used: placebo = 52; hormone = 16. n values represent the number of oocytes included. Statistical analysis for the metaphase II ploidy was done using a weighted two-tailed paired Welch t test. *$p < 0.05$ **$p < 0.01$, ***$p < 0.001$.

See also Figure S3.

of these findings is that long-term hormonal contraception can potentially ameliorate the maternal age effect.

Ovulation suppression in a pre-pubertal mouse model prevents chromosomal abnormalities in eggs

Both the successive pregnancies and the hormonal contraception models generate a hormonal environment akin to pregnancy, albeit presumably with distinct hormonal profiles and cycles. They both do not stop ovulations but merely reduce their frequency. A more definitive experiment would be to suppress ovulations without a pregnancy-like state. To achieve this, we engineered mice that undergo few or no ovulations. Ovulations are triggered by peaks in hormonal cycles in sexually mature females. The onset of sexual maturity is regulated by the G-protein coupled receptor (Gpr) 54, and mice lacking this receptor remain in a pre-pubescent state.[50] A rare genetic condition with mutations in *Gpr54* leads to idiopathic hypogonadotropic hypogonadism in humans.[50] We used CRISPR gene targeting to generate *Gpr54*$^{-/-}$ mice, which are infertile and lack signs of ovulation in the ovarian tissue, such as *corpora lutea* and pre-ovulatory follicles (Figures 6A and S4A–S4H), as reported previously. Because *Gpr54*$^{-/-}$ females lack pre-ovulatory follicles, it was necessary to hormone stimulate the mice to trigger oocyte growth (see STAR Methods).

To assess chromosomal abnormalities, we performed *in situ* fixation of eggs to capture all chromosomes. Since these mice are on a 129S2/SvHsd strain background, we determined the frequency of chromosomal abnormalities both in eggs from young (2-month-old) and aged (14- to 15-month-old) *Gpr54*$^{-/-}$ and *Gpr54*$^{+/+}$ female mice (Figure 6C). Chromosomal abnormalities in *Gpr54*$^{+/+}$ and *Gpr54*$^{-/-}$ eggs from young females occurred at frequencies of 4% and 5%, respectively ($p > 0.9$) (Figures 6D, 6E, S4I, and S4J). Importantly, the frequency of chromosomal abnormalities increased to 36% in eggs from aged *Gpr54*$^{+/+}$ females ($p = 0.0005$), but only to 17% in eggs from aged *Gpr54*$^{-/-}$ females (Figures 6D, 6E, S4I, and S4J). The increase in chromosomal abnormalities from 5% to 17% in *Gpr54*$^{-/-}$ oocytes from young versus aged females suggests that ovulation-independent aging also occurs ($p = 0.002$) (Figures 6D and 6E). However, the >2-fold reduction in chromosomal abnormalities in eggs from aged

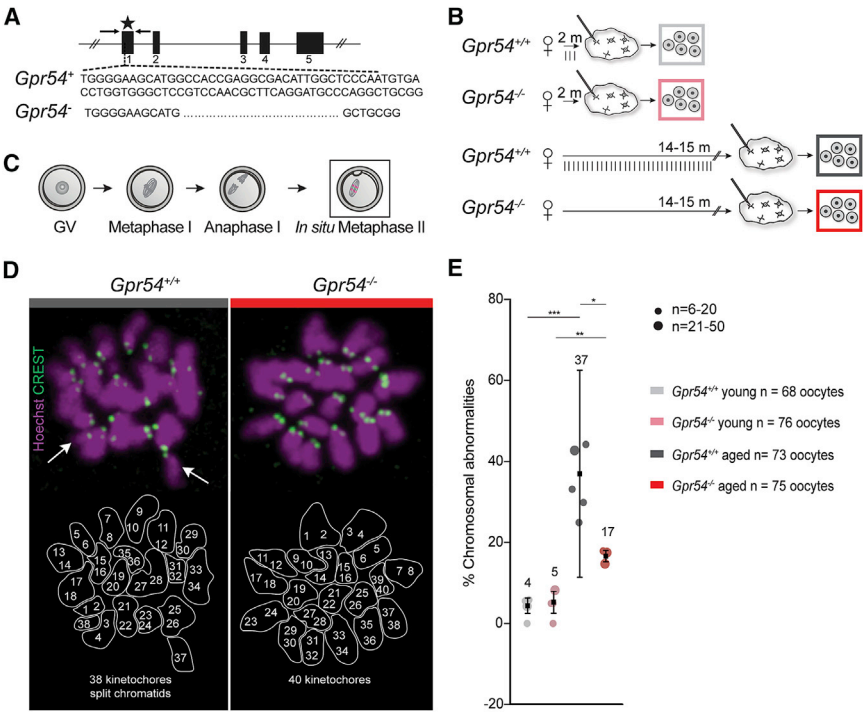

Figure 6. MII eggs from aged *Gpr54*$^{-/-}$ female mice show a reduction in chromosomal abnormalities

(A) CRISPR-Cas9 strategy generated a 67-bp frameshift deletion in exon 1 of *Gpr54*. Star represents the guide. Arrows represent the genotyping primer location.

(B) Oocyte retrieval from ovaries of virgin young and aged *Gpr54*$^{+/+}$ and *Gpr54*$^{-/-}$ mice after hormone priming (see STAR Methods) to induce oocyte maturation and ovulation. Vertical lines represent ovulations.

(C) Mature GV oocytes completed the meiosis I division *in vitro* and were fixed in meiosis II for immunofluorescent staining of kinetochores.

(D) Representative images of 3D reconstructions from the metaphase II plate of eggs paired with arithmetical representations of kinetochores. White arrows indicate split sister chromatids. DNA is stained with Hoechst dye and kinetochore proteins are detected with CREST antibody. Images generated with Fiji software. The chromosome area is marked by a line that encircles the numbered kinetochores. Scale bar, 5 μm.

(E) Incidence of chromosomal abnormalities in young and aged virgin *Gpr54*$^{+/+}$ and *Gpr54*$^{-/-}$ metaphase II oocytes (young versus aged *Gpr54*$^{+/+}$ p = 0.0005; young versus aged *Gpr54*$^{-/-}$ p = 0.002; aged *Gpr54*$^{+/+}$ versus *Gpr54*$^{-/-}$ p = 0.01). Individual circles represent separate experiments; the sizes vary according to the sample size of each experiment. Cubes represent the weighted mean of each condition with weighted SD error bars. Chromosomal abnormalities include any anomaly from 20 intact dyad chromosomes. Number of females used: young *Gpr54*$^{+/+}$ = 12; young *Gpr54*$^{-/-}$ = 12; aged *Gpr54*$^{+/+}$ = 48; and aged *Gpr54*$^{-/-}$ = 18. n values represent the number of oocytes included. Statistical analysis for the metaphase II ploidy was done using a weighted two-tailed paired Welch t test. *p < 0.05 **p < 0.01, ***p < 0.001, ****p < 0.0001.

See also Figure S4.

Gpr54$^{-/-}$ females suggests that ovulations, directly or indirectly, contribute to oocyte aging (Figure 6D) (p = 0.01).

DISCUSSION

The maternal age effect is thought to be due to physiological rather than chronological aging of oocytes.[51] An increase in meiotic chromosome segregation errors resulting in chromosomal abnormalities can be considered as a hallmark of aged oocytes and eggs. We provide evidence from three mouse models that the mechanisms for accurate chromosome segregation and production of euploid eggs can be protected until advanced maternal age. Each mouse model presented here—successive pregnancies, hormonal contraception, and pre-pubescence—has multiple effects on physiology, including presumably distinct endocrine changes, and is therefore individually insufficient for inferring the protective cause on oocyte aging. It is principally possible that the protection against oocyte aging is due to interfering with different mechanisms in each model, which would also be interesting and important to know. However, as will become apparent from the reasons outlined below, the most parsimonious explanation is that ovulation reduction protects against chromosomal abnormalities in eggs of aged females.

The mouse models have common features that could provide a unified explanation for the rescue in chromosome abnormalities with age. All three models have reduced ovulations and would therefore be expected to retain more oocytes in the ovary. We have not quantified oocyte numbers in tissue sections because this is technically incompatible with isolating oocytes for chromosome analysis, the primary focus, but would expect to find more oocytes per ovary in the mouse models compared to incessantly ovulating females. It has been proposed that a larger oocyte pool harbors "healthy" oocytes and that these are somehow selected for ovulation.[24] In addition to there being no mechanistic basis for the oocyte selection hypothesis, there is also no association between a naturally depleted oocyte pool and the incidence of trisomic pregnancies in humans.[25,26,52] Therefore, a larger oocyte pool would seem to be insufficient to explain a delay in oocyte aging.

Instead, we consider the commonality of reducing ovulations in the mouse models as relevant for the maternal age effect. Successive pregnancies and hormonal contraception resulted in a ~2-fold reduction of chromosomal abnormalities in eggs from aged females. If the protective effect was due to pregnancies or a pregnancy-like hormonal state (akin to contraception), then no protective effect would be expected for aging without pregnancies. Alternatively, if the protective effect was due to ovulation reduction, then suppressing ovulations in a way that does not imitate the hormonal state of pregnancy would also be expected to have a protective effect. Consistent with the latter, a >2-fold reduction in chromosomal abnormalities was detected in eggs from aged, pre-pubescent *Gpr54*$^{-/-}$ females, which undergo little or no ovulations. Another experimental

Table 1. Epidemiological studies on the effects of oral contraception on fecundity, incidence of miscarriage, and trisomies 13, 18, or 21

Purpose of Study	Time Elapsed Since Last Contraceptive Use	Positive	Negative	No Effect	Omitted Parameter	Study
Abortion risk	6 months		x		duration of oral contraceptive maternal age	58
Fecundity in breakthrough pregnancies	–		x		maternal age	59
Trisomy 21	12 months	x			duration of oral contraceptive	60
Trisomy 21	–			x	duration of oral contraceptive maternal age	61
Trisomy 21	–			x	duration of oral contraceptive	62
Miscarriage	–	x				63
Fecundity	6 months to >12 months	x			maternal age	64
Miscarriage	–		x		maternal age	65
Fecundity	–	x			maternal age	66
Trisomy 21	–	x				67
Trisomies 13, 18, and 21	–	x				68

A positive effect means oral contraceptive reduced the frequency of aneuploid pregnancies or miscarriages. A negative effect means that oral contraceptive increased the frequency of aneuploidy pregnancies or miscarriages. No effect means that oral contraceptive did not affect the frequency of aneuploid pregnancies or miscarriages.

condition to consider would be the subjection of mice to continuous rounds superovulation that would be predicted to lead to the early onset of the maternal age effect. Although it cannot be excluded that other processes such as tissue homeostasis contribute to the rescue in oocyte aging, these independent lines of evidence provide strong support for the hypothesis that ovulation frequency determines the physiological aging of oocytes.

An important consideration is whether human epidemiological studies support the hypothesis (Table 1). Studies of multiparous women, with up to 6 pregnancies, showed either no or adverse effects on pregnancy outcome.[53–55] This suggests that either 6 pregnancies are too few to have an impact on oocyte aging or variables other than the number of pregnancies matter (e.g., the timing of the first pregnancy and the spacing between pregnancies). Studies of women with more children are rare; however, an Amish population with an average fecundity of 10 children shows a miscarriage frequency of merely 10% at advanced maternal age.[56,57] This might suggest that high multiparity has a protective effect; however, it is not known whether there is an inherently lower frequency of miscarriages in this population.

Furthermore, oral contraception, which suppresses ovulation, would also be expected to reduce the risk of trisomic pregnancies and miscarriages, which are most commonly caused by fetal aneuploidy. There is no consensus on the effects of hormonal contraception on pregnancy outcome in the epidemiological literature. Early studies based on higher doses of combined estrogen/progesterone oral contraceptives showed negative effects on pregnancy outcome.[58,59,65] Oral contraception also has detrimental effects for pregnancies occurring during oral contraception (break-through pregnancies) or within 6 months after cessation of oral contraception; however, these studies did not take maternal age into consideration.[58,59,65] Some studies found no effect of oral contraception on trisomic pregnancies but did not consider the duration of oral contraception.[61,62] Recent studies based on moderate doses of combined oral contraceptives in human showed a positive effect on trisomic pregnancies, miscarriages, and fecundity.[60,63,64,66,68,69] Therefore, some support for the ovulation hypothesis can be found among epidemiological data, but the overall lack of consensus rendered it important to test itin an experimentally tractable system.

Some aspects of the maternal age effect cannot be explained by the ovulation hypothesis. These include the increase in aneuploidy incidence in early puberty, chromosome-specific incidence of trisomies, and the ovulation-independent increase in chromosomal abnormalities, as observed in *Gpr54*$^{-/-}$ females. Additional factors that contribute to the maternal age effect are meiotic recombination, which is already determined during fetal life, oxidative damage accumulation through natural aging,[70] and exposure to environmental toxins like BPA.[31]

The hypothesis that ovulations contribute to the maternal age effect can potentially also explain other phenomena. These include that the maternal age effect is rare in species that breed seasonally (seasonal ovulation) and naked mole rats can retain fertility over 2 decades by suppressing ovulation until becoming a queen.[71,72] Furthermore, dietary restrictions can reduce egg aneuploidy.[73] We interpret this finding in light of calorie restrictions also leading to ovulation suppression.

In addition, we have discovered that oocyte aging is accompanied by a change in 3D chromatin organization. Whether the increase in extruded loop size is mechanistically related to anaphase bridges is unclear. We speculate that longer loops may increase the likelihood of catenations between homologous chromosome arms in meiosis I, leading to entanglements that

manifest as anaphase bridges and result in aneuploidy. It is possible that other aging phenotypes and molecular mechanisms could also contribute to chromatin conformation changes that manifest in chromosome segregation defects during meiosis I. However, an interesting parallel occurs in somatic cells[47,48,74] and oocytes[43] lacking the cohesin release factor Wapl. Increasing cohesin residence time leads to longer loops and anaphase bridges in both cell types. It is therefore tempting to speculate that the loss of chromosomal Rec8 results in longer extruded loops and more anaphase bridges in oocytes from aged females.

To the extent that the mouse serves as an appropriate model for the maternal age effect,[19,21,27–29,39,75–83] our findings offer new perspectives on mammalian reproduction.[84] The data imply that ovulations are, directly or indirectly, a contributing cause to oocyte aging and the maternal age effect. Ovulation reduction can have a protective effect and delay oocyte aging. However, this benefit has to be carefully weighed against the known serious risks associated with hormonal contraception.[85–87] The mouse model investigated here used progesterone-only contraception, which mimics the "mini-pill" or "implant." To our knowledge, there are no reports on the long-term effects of progesterone-only contraception on aneuploid pregnancies. It will therefore be important to carry out further epidemiological studies on the improved hormonal contraceptive methods. Finally, our work implies that persistent superovulation would lead to an early maternal age effect onset, and long-term ovulation suppression could reduce the risk of egg aneuploidy at advanced maternal age.

STAR★METHODS

Detailed methods are provided in the online version of this paper and include the following:

- KEY RESOURCES TABLE
- RESOURCE AVAILABILITY
  - Lead contact
  - Materials availability
  - Data and code availability
- EXPERIMENTAL MODEL AND SUBJECT DETAILS
- METHOD DETAILS
  - Hormone priming
  - CRISPR/Cas9 and genotyping
  - Zygote retrieval and embryo transplantation
  - Surgical procedure
  - Retrieval and *in vitro* culturing of oocytes
  - Microinjection
  - Time-lapse microscopy
  - Chromosome spreads and *in situ* fixation
  - Immunofluorescence
  - Image acquisition
  - Paraffin sectioning and imaging
  - TEV protease cleavage assay
  - snHi-C sample acquisition
- QUANTIFICATION AND STATISTICAL ANALYSIS
  - Image analysis and quantification
  - Statistical analysis
  - snHi-C data analysis

SUPPLEMENTAL INFORMATION

Supplemental information can be found online at https://doi.org/10.1016/j.cub.2021.06.076.

ACKNOWLEDGMENTS

We are grateful to Jan-Michael Peters, William Henry Colledge, and Hugo Brandão for helpful advice. We would like to thank M. Herbert for kindly providing the C57BL/Icrf^{at} mouse strain and L. Chmátal and M. Lampson for sharing the 2xEGFP-CenpC plasmid and the Rec8 antibody, respectively. We thank H.C. Theussl and J. Wojciechowski (Transgenics facility) for CRISPR-Cas9 zygote injections, M. Zeba (histopathology facility) for tissue sectioning and staining, and the BioOptics facility for imaging advice. Illumina sequencing was performed at the VBCF NGS Unit and the NGS facility in the Department of Totipotency, MPIB. We thank T.R. Burkard from the IMP/IMBA bioinformatics facility for snHi-C statistical analysis support. We thank I. Gaspar for his advice on statistical analysis of the egg ploidy data. We are grateful to C. Schuh, K. Klien, S. Ladstätter, and A. Szydlowska-Bylicka for blind scoring of egg aneuploidy and the Tachibana lab for manuscript reading. We also thank Life Science Editors for editorial assistance. We would like to thank the funding bodies that support the research in the Tachibana lab. This work was funded by the Herzfelder Foundation (P 30613-B21) and the Austrian Science Fund (FWF). J.G. is supported by the L'Oréal Austria Fellowship for Women in Science. J.G. and B.J.H.D. are associated students of the DK Chromosome Dynamics (W1238-B20) supported by the Austrian Science Fund (FWF) and the European Research Council. Work in the Tachibana laboratory is supported by the European Research Council (ERC-StG0336460 ChromHeritance and ERC-CoG 818556 TotipotenZygotChrom), an HFSP project grant (RGP0057-2018), the Austrian Academy of Sciences, and the Max Planck Society.

AUTHOR CONTRIBUTIONS

Resources and Supervision, K.T.; Conceptualization, Funding Acquisition and Project Administration, K.T. and E.E.C.; Writing – Review & Editing, K.T. and E.E.C.; Visualization, E.E.C. (lead), S.P., and B.J.H.D. (supporting); Data Curation (all but HiC), E.E.C.; Formal analysis (all but HiC), E.E.C.; Investigation (all but HiC), E.E.C.; Methodology (all but HiC), E.E.C..; Writing – Original Draft, E.E.C.; Methodology and Investigation (HiC): J.G., B.J.H.D., and M.C.C.S.; Software, Data Curation, and Formal Analysis (HiC), S.P., B.J.H.D., and J.G.

DECLARATION OF INTERESTS

The authors declare no competing interests.

Received: March 9, 2020
Revised: April 1, 2021
Accepted: June 25, 2021
Published: July 26, 2021

REFERENCES

1. Hassold, T., and Chiu, D. (1985). Maternal age-specific rates of numerical chromosome abnormalities with special reference to trisomy. Hum. Genet. *70*, 11–17.
2. Kline, J., Kinney, A., Levin, B., and Warburton, D. (2000). Trisomic pregnancy and earlier age at menopause. Am. J. Hum. Genet. *67*, 395–404.
3. Koehler, K.E., Hawley, R.S., Sherman, S., and Hassold, T. (1996). Recombination and nondisjunction in humans and flies. Hum. Mol. Genet. *5*, 1495–1504.
4. Lamb, N.E., Freeman, S.B., Savage-Austin, A., Pettay, D., Taft, L., Hersey, J., Gu, Y., Shen, J., Saker, D., May, K.M., et al. (1996). Susceptible chiasmata configurations of chromosome 21 predispose to non-disjunction in both maternal meiosis I and meiosis II. Nat. Genet. *14*, 400–405.
5. Lamb, N.E., Feingold, E., Savage, A., Avramopoulos, D., Freeman, S., Gu, Y., Hallberg, A., Hersey, J., Karadima, G., Pettay, D., et al. (1997).

Characterization of Susceptible Chiasma Configurations that Increase the Risk for Maternal Nondisjunction of Chromosome 21 (Oxford University Press).

6. Hassold, T., and Hunt, P. (2001). To err (meiotically) is human: the genesis of human aneuploidy. Nat. Rev. Genet. *2*, 280–291.
7. Nagaoka, S.I., Hassold, T.J., and Hunt, P.A. (2012). Human aneuploidy: mechanisms and new insights into an age-old problem. Nat. Rev. Genet. *13*, 493–504.
8. Webster, A., and Schuh, M. (2017). Mechanisms of Aneuploidy in Human Eggs. Trends Cell Biol. *27*, 55–68.
9. Risch, N., Stein, Z., Kline, J., and Warburton, D. (1986). The Relationship between Maternal Age and Chromosome Size in Autosomal Trisomy. Am. J. Hum. Genet. *39*, 68–78.
10. Burkhardt, S., Borsos, M., Szydlowska, A., Godwin, J., Williams, S.A., Cohen, P.E., Hirota, T., Saitou, M., and Tachibana-Konwalski, K. (2016). Chromosome Cohesion Established by Rec8-Cohesin in Fetal Oocytes Is Maintained without Detectable Turnover in Oocytes Arrested for Months in Mice. Curr. Biol. *26*, 678–685.
11. Tachibana-Konwalski, K., Godwin, J., van der Weyden, L., Champion, L., Kudo, N.R., Adams, D.J., and Nasmyth, K. (2010). Rec8-containing cohesin maintains bivalents without turnover during the growing phase of mouse oocytes. Genes Dev. *24*, 2505–2516.
12. Lamb, N.E., Sherman, S.L., and Hassold, T.J. (2005). Effect of meiotic recombination on the production of aneuploid gametes in humans. Cytogenet. Genome Res. *111*, 250–255.
13. Wang, S., Kleckner, N., and Zhang, L. (2017). Crossover maturation inefficiency and aneuploidy in human female meiosis. Cell Cycle *16*, 1017–1019.
14. Wang, S., Hassold, T., Hunt, P., White, M.A., Zickler, D., Kleckner, N., and Zhang, L. (2017). Inefficient Crossover Maturation Underlies Elevated Aneuploidy in Human Female Meiosis. Cell *168*, 977–989.e17.
15. LeMaire-Adkins, R., Radke, K., and Hunt, P.A. (1997). Lack of checkpoint control at the metaphase/anaphase transition: a mechanism of meiotic nondisjunction in mammalian females. J. Cell Biol. *139*, 1611–1619.
16. Wassmann, K., Niault, T., and Maro, B. (2003). Metaphase I arrest upon activation of the Mad2-dependent spindle checkpoint in mouse oocytes. Curr. Biol. *13*, 1596–1608.
17. Kudo, N.R., Wassmann, K., Anger, M., Schuh, M., Wirth, K.G., Xu, H., Helmhart, W., Kudo, H., McKay, M., Maro, B., et al. (2006). Resolution of chiasmata in oocytes requires separase-mediated proteolysis. Cell *126*, 135–146.
18. McGuinness, B.E., Anger, M., Kouznetsova, A., Gil-Bernabé, A.M., Helmhart, W., Kudo, N.R., Wuensche, A., Taylor, S., Hoog, C., Novak, B., and Nasmyth, K. (2009). Regulation of APC/C activity in oocytes by a Bub1-dependent spindle assembly checkpoint. Curr. Biol. *19*, 369–380.
19. Kitajima, T.S., Ohsugi, M., and Ellenberg, J. (2011). Complete kinetochore tracking reveals error-prone homologous chromosome biorientation in mammalian oocytes. Cell *146*, 568–581.
20. Tachibana-Konwalski, K., Godwin, J., Borsos, M., Rattani, A., Adams, D.J., and Nasmyth, K. (2013). Spindle assembly checkpoint of oocytes depends on a kinetochore structure determined by cohesin in meiosis I. Curr. Biol. *23*, 2534–2539.
21. Holubcová, Z., Blayney, M., Elder, K., and Schuh, M. (2015). Human oocytes. Error-prone chromosome-mediated spindle assembly favors chromosome segregation defects in human oocytes. Science *348*, 1143–1147.
22. Vollenhoven, B., and Hunt, S. (2018). Ovarian ageing and the impact on female fertility. F1000Res *7*, F1000 Faculty Rev-1835.
23. Fu, X., Cheng, J., Hou, Y., and Zhu, S. (2014). The association between the oocyte pool and aneuploidy: a comparative study of the reproductive potential of young and aged mice. J. Assist. Reprod. Genet. *31*, 323–331.
24. Kline, J., Kinney, A., Reuss, M.L., Kelly, A., Levin, B., Ferin, M., and Warburton, D. (2004). Trisomic pregnancy and the oocyte pool. Hum. Reprod. *19*, 1633–1643.
25. Rowsey, R., Kashevarova, A., Murdoch, B., Dickenson, C., Woodruff, T., Cheng, E., Hunt, P., and Hassold, T. (2013). Germline mosaicism does not explain the maternal age effect on trisomy. Am. J. Med. Genet. A. *161A*, 2495–2503.
26. Warburton, D. (2005). Biological aging and the etiology of aneuploidy. Cytogenet. Genome Res. *111*, 266–272.
27. Hodges, C.A., Revenkova, E., Jessberger, R., Hassold, T.J., and Hunt, P.A. (2005). SMC1beta-deficient female mice provide evidence that cohesins are a missing link in age-related nondisjunction. Nat. Genet. *37*, 1351–1355.
28. Chiang, T., Duncan, F.E., Schindler, K., Schultz, R.M., and Lampson, M.A. (2010). Evidence that weakened centromere cohesion is a leading cause of age-related aneuploidy in oocytes. Curr. Biol. *20*, 1522–1528.
29. Lister, L.M., Kouznetsova, A., Hyslop, L.A., Kalleas, D., Pace, S.L., Barel, J.C., Nathan, A., Floros, V., Adelfalk, C., Watanabe, Y., et al. (2010). Age-related meiotic segregation errors in mammalian oocytes are preceded by depletion of cohesin and Sgo2. Curr. Biol. *20*, 1511–1521.
30. Revenkova, E., Herrmann, K., Adelfalk, C., and Jessberger, R. (2010). Oocyte cohesin expression restricted to predictyate stages provides full fertility and prevents aneuploidy. Curr. Biol. *20*, 1529–1533.
31. Hunt, P.A., Koehler, K.E., Susiarjo, M., Hodges, C.A., Ilagan, A., Voigt, R.C., Thomas, S., Thomas, B.F., and Hassold, T.J. (2003). Bisphenol a exposure causes meiotic aneuploidy in the female mouse. Curr. Biol. *13*, 546–553.
32. Nakamura, Y., Yamagata, Y., Sugino, N., Takayama, H., and Kato, H. (2002). Nitric oxide inhibits oocyte meiotic maturation. Biol. Reprod. *67*, 1588–1592.
33. Perkins, A.T., Das, T.M., Panzera, L.C., and Bickel, S.E. (2016). Oxidative stress in oocytes during midprophase induces premature loss of cohesion and chromosome segregation errors. Proc. Natl. Acad. Sci. USA *113*, E6823–E6830.
34. Espey, L.L. (1980). Ovulation as an inflammatory reaction–a hypothesis. Biol. Reprod. *22*, 73–106.
35. Murdoch, W.J., Townsend, R.S., and McDonnel, A.C. (2001). Ovulation-Induced DNA Damage in Ovarian Surface Epithelial Cells of Ewes: Prospective Regulatory Mechanisms of Repair/Survival and Apoptosis. BIOLOGY OF REPRODUCTION *65*, 1417–1424. https://doi.org/10.1095/biolreprod65.5.1417.
36. Yun, Y., Wei, Z., and Hunter, N. (2019). Maternal obesity enhances oocyte chromosome abnormalities associated with aging. Chromosoma *128*, 413–421.
37. Jia, Z., Feng, Z., Wang, L., Li, H., Wang, H., Xu, D., Zhao, X., Feng, D., and Feng, X. (2018). Resveratrol reverses the adverse effects of a diet-induced obese murine model on oocyte quality and zona pellucida softening. Food Funct. *9*, 2623–2633.
38. Zhang, L., Han, L., Ma, R., Hou, X., Yu, Y., Sun, S., Xu, Y., Schedl, T., Moley, K.H., and Wang, Q. (2015). Sirt3 prevents maternal obesity-associated oxidative stress and meiotic defects in mouse oocytes. Cell Cycle *14*, 2959–2968.
39. Kouznetsova, A., Kitajima, T.S., Brismar, H., and Höög, C. (2019). Post-metaphase correction of aberrant kinetochore-microtubule attachments in mammalian eggs. EMBO Rep. *20*, e47905.
40. Fudenberg, G., et al. (2016). Formation of Chromosomal Domains by Loop Extrusion. Cell Rep. *15*, 2038–2049. https://doi.org/10.1016/j.celrep.2016.04.085.
41. Lieberman-Aiden, Erez, et al. (2009). Comprehensive mapping of long-range interactions reveals folding principles of the human genome. Science *326*, 289–293. https://doi.org/10.1126/science.1181369.
42. Nora, Elphège, P., et al. (2017). Targeted Degradation of CTCF Decouples Local Insulation of Chromosome Domains from Genomic Compartmentalization. Cell *169*, 930–944.e22. https://doi.org/10.1016/j.cell.2017.05.004.
43. Silva, M.C., Powell, S., Ladstätter, S., Gassler, J., Stocsits, R., Tedeschi, A., Peters, J.-M., and Tachibana, K. (2020). Wapl releases Scc1-cohesin

and regulates chromosome structure and segregation in mouse oocytes. J. Cell Biol. *219*, e201906100.

44. Gassler, J., Brandão, H.B., Imakaev, M., Flyamer, I.M., Ladstätter, S., Bickmore, W.A., Peters, J.-M., Mirny, L.A., and Tachibana, K. (2017). A mechanism of cohesin-dependent loop extrusion organizes zygotic genome architecture. EMBO J. *36*, 3600–3618.
45. Dequeker, B.J.H., Brandão, H.B., Scherr, M.J., Gassler, J., Powell, S., Gaspar, I., Flyamer, I.M., Tang, W., Stocsits, R., Davidson, I.F., et al. (2020). MCM complexes are barriers that restrict cohesin-mediated loop extrusion. bioRxiv. https://doi.org/10.1101/2020.10.15.340356.
46. Davidson, I.F., Bauer, B., Goetz, D., Tang, W., Wutz, G., and Peters, J.M. (2019). DNA loop extrusion by human cohesin. Science *366*, 1338–1345.
47. Haarhuis, J.H.I., van der Weide, R.H., Blomen, V.A., Yáñez-Cuna, J.O., Amendola, M., van Ruiten, M.S., Krijger, P.H.L., Teunissen, H., Medema, R.H., van Steensel, B., et al. (2017). The Cohesin Release Factor WAPL Restricts Chromatin Loop Extension. Cell *169*, 693–707.e14.
48. Wutz, G., Várnai, C., Nagasaka, K., Cisneros, D.A., Stocsits, R.R., Tang, W., Schoenfelder, S., Jessberger, G., Muhar, M., Hossain, M.J., et al. (2017). Topologically associating domains and chromatin loops depend on cohesin and are regulated by CTCF, WAPL, and PDS5 proteins. EMBO J. *36*, 3573–3599.
49. Isono, W., Wada-Hiraike, O., Kawamura, Y., Fujii, T., Osuga, Y., and Kurihara, H. (2018). Administration of Oral Contraceptives Could Alleviate Age-Related Fertility Decline Possibly by Preventing Ovarian Damage in a Mouse Model. Reprod. Sci. *25*, 1413–1423.
50. Seminara, S.B., Messager, S., Chatzidaki, E.E., Thresher, R.R., Acierno, J.S., Jr., Shagoury, J.K., Bo-Abbas, Y., Kuohung, W., Schwinof, K.M., Hendrick, A.G., et al. (2003). The GPR54 gene as a regulator of puberty. N. Engl. J. Med. *349*, 1614–1627.
51. Hunt, P., and Hassold, T. (2010). Female meiosis: coming unglued with age. Curr. Biol. *20*, R699–R702.
52. Kline, J.K., Kinney, A.M., Levin, B., Kelly, A.C., Ferin, M., and Warburton, D. (2011). Trisomic pregnancy and elevated FSH: implications for the oocyte pool hypothesis. Hum. Reprod. *26*, 1537–1550.
53. Chan, A., McCaul, K.A., Keane, R.J., and Haan, E.A. (1998). Effect of parity, gravidity, previous miscarriage, and age on risk of Down's syndrome: population based study. BMJ *317*, 923–924.
54. Doria-Rose, V.P., Kim, H.S., Augustine, E.T.J., and Edwards, K.L. (2003). Parity and the risk of Down's syndrome. Am. J. Epidemiol. *158*, 503–508.
55. Schimmel, M.S., Eidelman, A.I., Zadka, P., Kornbluth, E., and Hammerman, C. (1997). Increased parity and risk of trisomy 21: review of 37,110 live births. BMJ *314*, 720–721.
56. Cross, H.E., and McKusick, V.A. (1970). Amish demography. Soc. Biol. *17*, 83–101.
57. Resseguie, L.J. (1974). Pregnancy wastage and age of mother among the Amish. Hum. Biol. *46*, 633–639.
58. Carr, D.H. (1970). Chromosome studies in selected spontaneous abortions. 1. Conception after oral contraceptives. Can. Med. Assoc. J. *103*, 343–348.
59. Harlap, S., and Eldor, J. (1980). Births following oral contraceptive failures. Obstet. Gynecol. *55*, 447–452.
60. Janerich, D.T., Flink, E.M., and Keogh, M.D. (1976). Down's syndrome and oral contraceptive usage. Br. J. Obstet. Gynaecol. *83*, 617–620.
61. Ericson, A., Källén, B., and Lindsten, J. (1983). Lack of correlation between contraceptive pills and Down's syndrome. Acta Obstet. Gynecol. Scand. *62*, 511–514.
62. Källén, B. (1989). Maternal use of oral contraceptives and Down syndrome. Contraception *39*, 503–506.
63. Ford, J.H., and MacCormac, L. (1995). Pregnancy and lifestyle study: the long-term use of the contraceptive pill and the risk of age-related miscarriage. Hum. Reprod. *10*, 1397–1402.
64. Farrow, A., Hull, M.G., Northstone, K., Taylor, H., Ford, W.C., and Golding, J. (2002). Prolonged use of oral contraception before a planned pregnancy is associated with a decreased risk of delayed conception. Hum. Reprod. *17*, 2754–2761.
65. García-Enguídanos, A., Martínez, D., Calle, M.E., Luna, S., Valero de Bernabé, J., and Domínguez-Rojas, V. (2005). Long-term use of oral contraceptives increases the risk of miscarriage. Fertil. Steril. *83*, 1864–1866.
66. Mikkelsen, E.M., Riis, A.H., Wise, L.A., Hatch, E.E., Rothman, K.J., and Sørensen, H.T. (2013). Pre-gravid oral contraceptive use and time to pregnancy: a Danish prospective cohort study. Hum. Reprod. *28*, 1398–1405.
67. Nagy, G.R., Győrffy, B., Nagy, B., and Rigó, J. (2013). Lower risk for Down syndrome associated with longer oral contraceptive use: a case-control study of women of advanced maternal age presenting for prenatal diagnosis. Contraception *87*, 455–458.
68. Horányi, D., Babay, L.É., Rigó, J., Jr., Győrffy, B., and Nagy, G.R. (2017). Effect of extended oral contraception use on the prevalence of fetal trisomy 21 in women aged at least 35 years. Int. J. Gynaecol. Obstet. *138*, 261–266.
69. Nagy, G.R., Győrffy, B., Nagy, B., and Rigó, J., Jr. (2013). Lower risk for Down syndrome associated with longer oral contraceptive use: a case-control study of women of advanced maternal age presenting for prenatal diagnosis. Contraception *87*, 455–458.
70. Harman, D. (1956). Aging: a theory based on free radical and radiation chemistry. J. Gerontol. *11*, 298–300.
71. Buffenstein, R. (2005). The naked mole-rat: a new long-living model for human aging research. J. Gerontol. A Biol. Sci. Med. Sci. *60*, 1369–1377.
72. Jarvis, J.U. (1981). Eusociality in a mammal: cooperative breeding in naked mole-rat colonies. Science *212*, 571–573.
73. Selesniemi, K., Lee, H.-J., Muhlhauser, A., and Tilly, J.L. (2011). Prevention of maternal aging-associated oocyte aneuploidy and meiotic spindle defects in mice by dietary and genetic strategies. Proc. Natl. Acad. Sci. USA *108*, 12319–12324.
74. Tedeschi, A., Wutz, G., Huet, S., Jaritz, M., Wuensche, A., Schirghuber, E., Davidson, I.F., Tang, W., Cisneros, D.A., Bhaskara, V., et al. (2013). Wapl is an essential regulator of chromatin structure and chromosome segregation. Nature *501*, 564–568.
75. Nagaoka, S.I., Hodges, C.A., Albertini, D.F., and Hunt, P.A. (2011). Oocyte-specific differences in cell-cycle control create an innate susceptibility to meiotic errors. Curr. Biol. *21*, 651–657.
76. Chiang, T., Schultz, R.M., and Lampson, M.A. (2011). Age-dependent susceptibility of chromosome cohesion to premature separase activation in mouse oocytes. Biol. Reprod. *85*, 1279–1283.
77. Shomper, M., Lappa, C., and FitzHarris, G. (2014). Kinetochore microtubule establishment is defective in oocytes from aged mice. Cell Cycle *13*, 1171–1179.
78. Yun, Y., Lane, S.I.R., and Jones, K.T. (2014). Premature dyad separation in meiosis II is the major segregation error with maternal age in mouse oocytes. Development *141*, 199–208.
79. Zielinska, A.P., Holubcova, Z., Blayney, M., Elder, K., and Schuh, M. (2015). Sister kinetochore splitting and precocious disintegration of bivalents could explain the maternal age effect. eLife *4*, e11389.
80. Nakagawa, S., and FitzHarris, G. (2017). Intrinsically Defective Microtubule Dynamics Contribute to Age-Related Chromosome Segregation Errors in Mouse Oocyte Meiosis-I. Curr. Biol. *27*, 1040–1047.
81. Sakakibara, Y., Hashimoto, S., Nakaoka, Y., Kouznetsova, A., Höög, C., and Kitajima, T.S. (2015). Bivalent separation into univalents precedes age-related meiosis I errors in oocytes. Nat. Commun. *6*, 7550.
82. Nabti, I., Grimes, R., Sarna, H., Marangos, P., and Carroll, J. (2017). Maternal age-dependent APC/C-mediated decrease in securin causes premature sister chromatid separation in meiosis II. Nat. Commun. *8*, 15346.
83. Schuh, M., and Ellenberg, J. (2008). A new model for asymmetric spindle positioning in mouse oocytes. Curr. Biol. *18*, 1986–1992.
84. Mak, I.W., Evaniew, N., and Ghert, M. (2014). Lost in translation: animal models and clinical trials in cancer treatment. Am. J. Transl. Res. *6*, 114–118.

85. Kumle, M., Weiderpass, E., Braaten, T., Persson, I., Adami, H.-O., and Lund, E. (2002). Use of oral contraceptives and breast cancer risk: The Norwegian-Swedish Women's Lifestyle and Health Cohort Study. Cancer Epidemiol. Biomarkers Prev. *11*, 1375–1381.

86. Gadducci, A., Barsotti, C., Cosio, S., Domenici, L., and Riccardo Genazzani, A. (2011). Smoking habit, immune suppression, oral contraceptive use, and hormone replacement therapy use and cervical carcinogenesis: a review of the literature. Gynecol. Endocrinol. *27*, 597–604.

87. Peck, R., and Norris, C.W. (2013). Significant Risks of Oral Contraceptives (OCPs): Why This Drug Class Should Not Be Included in a Preventive Care Mandate. Linacre Q. *79*, 41–56.

88. Edgar, R., Domrachev, M., and Lash, A.E. (2002). Gene Expression Omnibus: NCBI gene expression and hybridization array data repository. Nucleic Acids Res. *30*, 207–210.

89. Rowlatt, C., Chesterman, F.C., and Sheriff, M.U. (1976). Lifespan, age changes and tumour incidence in an ageing C57BL mouse colony. Lab. Anim. *10*, 419–442.

90. Rabut, G., and Ellenberg, J. (2004). Automatic real-time three-dimensional cell tracking by fluorescence microscopy. J. Microsc. *216*, 131–137.

91. Flyamer, I.M., Gassler, J., Imakaev, M., Brandão, H.B., Ulianov, S.V., Abdennur, N., Razin, S.V., Mirny, L.A., and Tachibana-Konwalski, K. (2017). Single-nucleus Hi-C reveals unique chromatin reorganization at oocyte-to-zygote transition. Nature *544*, 110–114.

STAR★METHODS

KEY RESOURCES TABLE

REAGENT or RESOURCE	SOURCE	IDENTIFIER
Antibodies		
Anti-Crest	In house/Antibodies Incorporated	N/A/Cat. No #15-235-0001; RRID:AB_2797146
Anti-Rec8	Abcam	Cat. No #ab192241
Alexa Fluor® goat anti-rabbit 488	Invitrogen	Cat. No #A11008; RRID: AB_143165
Alexa Fluor® goat anti-human 594	Invitrogen	Cat. No #A11014 RRID:AB_2534081
Bacterial and virus strains		
STBL3 *E.coli*	In house	N/A
Chemicals, peptides, and recombinant proteins		
BSA	Sigma	Cat. No #A4503-100G
Phusion polymerase	NEB/in house	Cat. No #M0530L/ N/A
Goat serum	Dako	Cat. No #X0907
FBS	Invitrogen	Cat. No #10438026
DTT (for chromosome spread)	Sigma	Cat. No #43816-50ML
PMSG	Intervet Austria/Prospecbio	Cat. No #Folligon 1000I.E., / #HOR-272
hCG	Intervet Austria	Cat. No #Chorulon 1500 I.E.
Hyaluronidase	Sigma	Cat. No #H3506
KSOM medium	Merck/Millipore	Cat. No # MR-020P-5F
3-Isobutyl-1-methylxanthine (IBMX)	Sigma	Cat. No #I7018
N6,2'-O'Dibutyryl-adenosin-3', 5'-cyclophosphat	Sigma	Cat.D0627
M2 medium	In house	N/A
M16 medium	In house	N/A
Mineral oil	Sigma	Cat. No #M8410-500ML
EmbryoMax® Filtered Light Mineral Oil	Millipore	Cat. No #ES-005-C
Acidic Tyrode's solution	Sigma	Cat. No #T1788
FA (for *in situ* staining)	Thermo Scientific	Cat. No #28908
Formalin 10%	VWR	Cat. # FOR0020AF59001
PFA (for chromosome spread)	Sigma	Cat. No #158127-500G
RNase free water	Ambion	Cat. No #AM9939
BbsI	NEB	Cat. No #R0539S
SDS	Sigma	Cat. No #L6026-50G
Tween 20	Sigma	Cat. No #P7949
Triton X-100	Sigma	Cat. No #T8787-250ml
Vectashield® plus Dapi	Vector Labs	Cat. No #H-1200
Vectashield®	Vector Labs	Cat. No # H-1000
Hoechst	Invitrogen	Cat. No # H3570
Critical commercial assays		
PCR Purification Kit	QIAGEN	Cat. No #NA1020
mMESSAGE mMACHINE® T7 ULTRA Transcription Kit	Ambion	Cat. No #AM1345
MEGAshortscript T7 Transcription Kit	Ambion	Cat. No #AM1354
MEGAclear Transcription Clean-Up Kit	Ambion	Cat. No #AM1908
TA cloning kit	Invitrogen	Cat. No #K2020-40
Ketasol 100mg/ml	AniMedica	N/A
Xylazine 20mg/ml	AniMedica	N/A

(*Continued on next page*)

Continued

REAGENT or RESOURCE	SOURCE	IDENTIFIER
Deposited data		
Single nucleus Hi-C samples	GEO repository	Series GSE171159 https://www.ncbi.nlm.nih.gov/geo/query/acc.cgi?acc=GSE171159
Chromatin conformation capture data scripts	Zenodo	[Zenodo]:[https://doi.org/10.5281/zenodo.4917196 https://zenodo.org/record/4917196#.YMNqQjYzbp4]
Experimental models: organisms/strains		
C57BL/Icrf^{at}	M. Herbert, Newcastle University, Newcastle Fertility Centre, International Centre of Life, UK	N/A
C57BL/6J	IMBA, IMP Animal House facility, Vienna, Austria	N/A
129S2/SvHsd	Harlan, Indianapolis, IN, USA	N/A
Rec8$^{TEV/TEV}$	Kim Nasmyth, Department of Biochemistry, Univeristy of Oxford, UK	N/A
Wapl$^{fl/fl}$	Antonio Tedeschi, Institute of Molecular Pathology, Vienna Biocenter, Vienna, AT	N/A
(Tg)Zp3-Cre	Barbara B Knowles, The Jackson Laboratory, Bar Harbor, USA	N/A
Oligonucleotides		
5'-GGCTCCGTCCAACGCTTC-3'	Sigma	N/A
5'-TAATACGACTCACTATAG GGAGAATGGACTATAAGG ACCACGAC-3'	Sigma	N/A
5'- TAATACGACTCACTATAGG CTCCGTCCAACGCTTC-3'	Sigma	N/A
5'-AAACGAAGCGTTGGACGGA GCC-3'	Sigma	N/A
5'–GCGAAGCTAGCAGAGGA GCCTCTTTCC–3'	Sigma	N/A
5'-AGATGACCAATGAGTTT CCGACCAGCC-3'	Sigma	N/A
Recombinant DNA		
pX330 vector	Addgene	Cat. No #42230
Software and algorithms		
R studio Version 1.4	The R Foundation for Statistical computing	https://www.rstudio.com/products/rstudio/download/preview/
Weights: Weighting and Weighted Statistic, Version 1.0.4	The R Foundation for Statistical computing	https://cran.r-project.org/web/packages/weights/weights.pdf https://cran.r-project.org/web/packages/weights/index.html
MIT CRISPR Design Tool	F. Zhang lab, MIT	https://zlab.bio/guide-design-resources
ImageJ/Fiji Version 1.53	NIH, USA	https://imagej.nih.gov/ij/notes.html
GraphPad Prism, Version 7.00 for Mac OS X	GraphPad Software, La Jolla California USA	https://www.graphpad.com:443/
Imaris Versions from ± 8	Bitplane	https://imaris.oxinst.com/support/imaris-release-notes/8-0-0
Microsoft Excel, Version 16.43.1	Microsoft	https://www.microsoft.com/en-us/microsoft-365/excel

RESOURCE AVAILABILITY

Lead contact

Further information and requests for resources and reagents should be directed to and will be fulfilled by the Lead Contact, Kikuë Tachibana (tachibana@biochem.mpg.de).

Materials availability

Mouse lines generated in this study are available upon request.

Data and code availability

- The chromatin conformation capture data have been deposited in NCBI's Gene Expression Omnibus[88] and are accessible through GEO and are publicly available as of the date of publication. The accession numbers are listed in the Key resources table.

Microscopy data reported in this paper will be shared by the lead contact upon request.

- Data reported in this paper will be shared by the lead contact upon request.
- The snHi-C processing pipeline has been deposited at Zenodo and is publicly available as of the date of publication. The DOI is listed in the Key resources table.

Any additional information required to reanalyze the data reported in this paper is available from the lead contat upon request.

EXPERIMENTAL MODEL AND SUBJECT DETAILS

The *Gpr54* knockout mouse strain was generated on a 129S2/SvHsd background from Harlan. *Gpr54* control and experimental mice were obtained from heterozygous (*Gpr54*$^{+/-}$) crosses. Young females were 2 months old and aged females were 14-15 months old. The total number of mice used with the *Gpr54* pre-pubescent model is: young *Gpr54*$^{+/+}$ = 12; young *Gpr54*$^{-/-}$ = 12; aged *Gpr54*$^{+/+}$ = 48; aged *Gpr54*$^{-/-}$ = 18.

The C57BL/Icrf^{at} strain was used for ovulation reduction experiments by constant mating and hormonal contraception since the mice are free from specific age-associated pathologies.[89] C57BL/Icrf^{at} strain was maintained by wild-type crosses. Cages of experimental control mice were supplemented with male bedding from 8 months onward to support continued cyclicity, which was examined at two separate time points during the aging process by performing sequential vaginal smears over a period of 4 days to determine a full oestrus cycle. Females used for the constant mating and hormonal contraception experimental conditions were randomly (simple randomization) selected from litters of 4 to 6 females. The remaining females were used as controls. The necessity to perform many experiments over a period of year(s) contributes to, at least partial, overcoming of nuisance variables. Young females were 2 months old and aged females were 14-15 months old. The total number of mice used for the C57BL/Icrf^{at} hormonal contraception and placebo model is: placebo = 47; hormone = 13. The total number of mice used for the C57BL/Icrf^{at} for live cell imaging model is: young virgin = 16; aged virgin = 31; aged mated = 18. The total number of mice used for the C57BL/Icrf^{at} for metaphase II chromosome spreads experiment is: young virgin = 12; aged virgin = 53; aged mated = 23. The total number of mice used for the C57BL/Icrf^{at} for Rec8 quantification *in situ* and metaphase I chromosome spread experiments is: young virgin = 4; aged virgin = 34; aged mated = 11.

For the snHiC experiment of young and aged oocytes, 2-2.5-month-old and 14-18-month-old C57BL/6J (IMBA animal house) females were used. The C57BL/6J strain was maintained by wild-type crosses. The total number of C57BL/6J mice used for snHiC is: young = 7; aged = 12. C57BL/Icrf^{at} for snHiC young = 3; aged virgin = 7; aged mated = 2. The *Rec8*$^{TEV/TEV}$*Wapl*$^{fl/fl}$ *(Tg)Zp3*-Cre (C57BL/6J;129SV/Hsd;CBA) mice were generated by first breeding of *Wapl*$^{fl/fl}$ with hemizygous *(Tg)Zp3*-Cre males (unknown strain background) followed by breeding of *Wapl*$^{fl/fl}$ *(Tg)Zp3*-Cre males with *Rec8*$^{TEV/TEV}$ females (see further information on the strains in the Key resources table). The *Rec8*$^{TEV/TEV}$ and *Wapl*$^{fl/fl}$ strains are maintained on a mixed BL6/129Sv/CBA background. The total number of mice used for the *Rec8*$^{TEV/TEV}$*Wapl*$^{fl/fl}$ *(Tg)Zp3*-Cre (C57BL/6J;129SV/Hsd;CBA) snHiC experiments is: 6.

All animal experiments were carried out in agreement with the authorizing committee of the Institute of Molecular Biotechnology of the Austrian Academy of Sciences (IMBA, Vienna, Austria) according to the Austrian Animal Welfare law and the international guiding principles for biomedical research involving animals (CIOMS, the Council for International Organizations of Medical Sciences).

Mice were housed under a 14h light/10h dark cycle in individually ventilated cages with continuous access to food and water. Animals were housed grouped (maximum 5 males per cage and maximum 6 females per cage). During the aging process, mice which had to be sacrificed due to illness or were found dead, were not replaced by age-matched mice, therefore the number of mice per cage varied due to litter size and age. Mice which were to be weaned at the same time, were grouped to ensure sufficient mice were present in each cage and to save on resources.

Sample sizes depend on the number of oocytes yielded from the available test mice and controls used. We retrieved as many oocytes as possible per condition to address all the experiments we present here and all experiments that were necessary to optimize

the techniques used. It is challenging to reach large numbers of cells per condition[4,6] due to the fact that oocyte retrieval from aged mice oftens results in very few and even no oocytes, which are often not mature enough. Mice were littermates whenever possible or age-matched mice. Wild-type strain mice were randomly assigned for pellet implanation or aging. Mice which upon ovarian extraction were found to have tumor(s), a large spleen or were obviously sick were not used. Mice in the constant mating experimental condition were housed with a male from 2 m of age until approximately 1 m prior to hormone priming for oocyte retrieval. In the cases where signs of pregnancy were evident, these mice were excluded from the experiment. Oocytes which did not fulfill maturity criteria were excluded. In particular, oocytes from the aged but also young C57BL/Icrf^{at} mice were considered mature when most of the maturity criteria were fulfilled (oocyte size, GV position, thickness and smoothness of the zona pellucida). Oocytes from the C57BL/Icrf^{at} and C57BL/6J strains were permitted 2 hr for germinal vesicle breakdown (GVBD) breakdown whereas oocytes from the *Gpr54* strain where permitted 90 min. Oocytes which appeared to have non-surrounded nucleolus during live cell imaging, regardless of whether they completed GVBC on time, were excluded. Animals which were used for pellet implantation under anesthesia were maintained on a warm plate until they woke up from anesthesia as evidenced by the presence of urination and movement. They were then transferred to their cage under observation until they completely recovered from the procedure. Chromosome spreads which appeared spead out where not included in the analysis due to possible false positive or negative result. N number in the text, figures and figure legends refers to the number of cells included unless otherwise stated.

METHOD DETAILS

Hormone priming

Young mice were hormone primed with 5 IU (2 month) and aged mice with 7.5 IU of pregnant mare's serum gonadotropin (PMS, Intervet Austria) when superovulated. *Gpr54*$^{-/-}$ where stimulated once per week for three weeks and sacrificed 44-48 hr following the last PMS injection.

CRISPR/Cas9 and genotyping

The MIT CRISPR Design Tool from F. Zhang lab (https://zlab.bio/guide-design-resources) was used for guide RNA design. *Exon 1* of *GPR54* was targeted using 5'-GGCTCCGTCCAACGCTTC-3'. A T7 promoter was added to *Cas9* cDNA by PCR amplification of pX330, using primers 5'-TAATACGACTCACTATAGGGAGAATGGACTATAAGGACCACGAC-' and 5'-GCGAGCTCTAGGAATT CTTAC-3'. Purified *T7-Cas9* PCR product was used as template for *in vitro* transcription (IVT) using mMESSAGE mMACHINE T7 ULTRA kit (Life Technologies).

Oligos, designed with *Bbs*I overhangs, were phosphorylated, annealed, ligated into *Bbs*I digested, dephosphorylated pX330 vector and transformed into STBL3 *E. coli.* T7 IVT template was produced with a T7 promoter sequence containing primers '- TAATAC GACTCACTATAGGCTCCGTCCAACGCTTC-3' and 5'-AAACGAAGCGTTGGACGGAGCC-3'. Purified T7-sgRNA PCR product was used as a template for *in vitro* transcription with MEGAshortscript T7 Transcription Kit (Life Technologies). Cas9 mRNA and guide RNA were purified using the MEGAclear kit (Life Technologies) and eluted in RNase-free water.

Genotyping was performed primers: 5'–GCGAAGCTAGCAGAGGAGCCTCTTTCC–3' and 5'-AGATGACCAATGAGTTTCCGAC CAGCC-3'. Product sizes of *GPR54*$^{+}$ are 376 bp of *GPR54*$^{-}$ are 309 bp.

Zygote retrieval and embryo transplantation

For zygote retrieval for the generation of the *Gpr54* knockout mice, timed mating was performed with 3-5 week-old female mice superovulated by consecutive intraperitoneal injections of 5 U pregnant mare's serum (PMS, Intervet Austria) followed by 5 U of human chorionic gonadotropin (hCG, Intervet Austria) 48 h later. The second injection is used as reference time point for all experiments (time post-superovulation). Females were sacrificed 17-18 h post-hCG. Zygotes were released from cumulus cells by brief incubation with 300 μg/ml hyaluronidase (Sigma-Aldrich). Cells were cultured in ~40 μL drops of KSOM media (Milipore) covered with mineral oil or EmbryoMax® Filtered Light Mineral Oil (Sigma or Milipore, respectively) and incubated at 37°C and 5% CO2. A freshly prepared mix of 100 ng/μl of Cas9 mRNA, 50 ng/μl sgRNA was microinjected into cytoplasm of pronuclear-stage zygotes. Zygotes were cultured until the 2-cell stage and transferred into oviducts of pseudopregnant 129S2/SvHsd females.

Surgical procedure

Medroxyprogesterone- and placebo- containing 90 day slow-release pellets from Innovative Research of America (10mg of medroxyprogesterone acetate or no hormone) were implanted after anesthesia with Ketamine/Xylazine mix (17.5mg/ml Ketamine/2.5mg/ml Xylazine mix in saline buffer; dosage: 0.1ml intraperitoneally per 20 g mouse) at 2 months of age on the back of the mice subcutaneously. Anesthetic plane was evaluated by testing reaction to toe pinch. Anaesthesia lasted for 20-30 min. Mice which did not respond to anesthesia were terminated. The procedure was repeated at 5 months and 8 months. To verify ovulation suppression, hormone implanted mice were placed in mating with stud males for the duration of the treatment and did not get pregnant until 4 months after the final pellet was inserted.

Retrieval and *in vitro* culturing of oocytes

Fully grown oocytes, naturally arrested in dictyate of prophase I, were isolated by physical disaggregation of ovaries from appropriately aged females in M2 medium supplemented with 0.2 mM of the phosphodiesterase inhibitor 3-Isobutyl-1-methylxanthine or

0.25mM N6,2¢-O'Dibutyryl-adenosin-3¢, 5¢-cyclophosphate (IBMX or dbcAMP, both from Sigma-Aldrich) at 37°C. Mature oocytes were selected according to appearance (size, central nucleus, smooth zona pellucida) and cultured in M16 media supplemented with IBMX at 37°C and 5% CO2. Resumption of meiosis I was triggered by wash out of IBMX and successive culturing in M16 media. Timely nuclear envelope breakdown within 90 min, for the 129S2/SvHsd and *Rec8*$^{TEV/TEV}$ *Wapl*$^{\Delta/\Delta}$ strains and 120 min for all other strains, post-release from IBMX was used as further indicator of oocyte maturity. Oocyte cultivation was performed in ~40 μL drops covered with mineral oil (Sigma- Aldrich).

Microinjection

Microinjection of *in vitro* transcribed mRNA dissolved in RNase-free water (mMessage mMachine T3 kit, Ambion) was performed in M2 media using a Pneumatic PicoPump (World Precision Instruments) and hydraulic micromanipulator (Narishige) mounted onto a Zeiss Axiovert 200 microscope equipped with a 10x/0.3 EC plan-neofluar and 40x/0.6 LD Apochromat objective. Capped mRNA constructs with a 30 poly-A tail were synthesized using a T3 and T7 mMESSAGEmMACHINE kit (Ambion) from plasmids H2B-mCherry and 2xeGFP-CenpC (a gift from Lukáš Chmátal, Michael Lampson lab, University of Pennsylvania), respectively.

Time-lapse microscopy

A customized Zeiss LSM510 META confocal microscope equipped with PC-Apochromat 63x/1.2 NA water immersion objective lens was used for high-resolution live cell image acquisition (37°C incubator buffered with 5% CO_2). Cells were mounted to the microscope using Thermo ScientificTM NuncTM Lab-TekTM Chambered Coverglass (Fisher Scientific) and incubated in M16 media covered with mineral oil (Sigma-Aldrich) at 37°C and 5% CO2. Chromosomes labeled with H2B-mCherry were tracked with an EMBL-developed tracking macro adapted to the microscope.[90] Image stacks of 11 slices of 2 μm were captured every 20 min for 20 h. Final images of 0.25 μm z stacks were collected from oocytes that had completed meiosis I for 3D reconstruction of the metaphase II spindle for quantification of chromosomes and kinetochores. Metaphase I errors were scored one time frame prior to anaphase (time stamps h:min from GVBD). Oocytes from young virgin females progressed from GV breakdown through the meiosis I division (polar body extrusion, PBE) in 9 h 48 min ± 1 h 35 min (n = 49 cells). In contrast, oocytes from aged virgin females progressed to PBE in 12 h 42 min ± 1 h 54 min (n = 37 cells), with delayed kinetics compared to oocytes from young virgin females. Oocytes from aged mated females divided at 11 h 12 min ± 1 h 30 min (n = 42 cells), suggesting that reduced ovulation frequency partially restores the timely progression of meiosis I in aged females.

Chromosome spreads and *in situ* fixation

Mature GV oocytes that resumed meiosis by germinal vesicle breakdown (GVDB) within 1.5 h for the 129S2/SvHsd strain and 2 h for the C57BL/Icrf^{at} strain were used for experiments. Spreads were performed as described previously.[11] For Metaphase I spreads, oocytes were washed through Acidic Tyrode's buffer (pH 2.5, Sigma)) at 37°C to remove the zona pellucida at 5.5 h post-release from IBMX. Few oocytes were processed at a time to avoid dilution of Acidic Tyrode's buffer with M2 media that could result in incomplete zona pellucida removal. When the zona pellucida appeared to be fully removed, oocytes were quickly transferred to M2 for 3 sequential washes. Cells were then placed in recovery in 1:1 FBS(Sigma):dH_2O at 37°C for 14 min. 5.5h post release cells were spread into drops of freshly prepared 1% PFA solution (Sigma) pH 9.2-9.3 supplemented with 0.15% Triton X-100 (Sigma) and 3 mM DTT (Sigma). Slides were air-dried and frozen in −80 degrees for further antibody staining. The same method was applied for Metaphase II spreads.

For further processing, the slides were thawed, washed with 0.08% Kodak Professional Photo-Flo 200 solution (Kodak), 1x PBS and Immuno-washing solution (0.2% BSA, 0.1% Tween 20 (Sigma) in 1x PBS), followed by blocking with 10% goat serum (Dako), 2.5% BSA, 0.1% Tween 20 in 1xPBS.

For Metaphase I *in situ*, oocytes were collected 6 hr post GVBD and fixed in 2% FA (in 0.5 x PBS with 25 mM HEPES, Thermo Scientific) supplemented with 0.1% Triton X-100 for 30 min at room temperature in a humidified chamber. Cells were permeabilized with 0.1% Triton X-100 in PBS for 15 min at room temperature. At this stage cells were either directly processed or stored for future staining to pool cell numbers per staining and imaging experiment. For storage purposes, cells were passed through increasing concentrations of mounting media mixed in blocking solotuion until 100% mounting media (Vectashield). They were then stored in mouth pipettes at −20C until further processing. When thawed, they were washed in three drops of 0.1% Triton X-100 for 10 min each, before proceeding with blocking (0.3% BSA prepared freshly in PBS with 0.01% Tween20) and staining. For direct processing cells were placed in blocking solution for 2 hr or overnight at 4°C in a humidified chamber. Washes after primary and secondary staining (3x 30 min at room temperature or overnight) were performed in blocking solution.

Immunofluorescence

Immunofluorescent staining was performed with anti-Rec8 (for chromosome spreads: 1:50, Abcam, ab192241; for MI *in situ*: 1:1000 Lampson lab Rec8 Ab gift) and CREST (1:500, a gift from Jan-Michael Peters, IMP and Antibodies Incorporated, 15-235-0001) antibodies in blocking solution overnight at 4°C in a humidified chamber. Alexa Fluor® goat anti-human 594 (1:500) and goat anti-rabbit 488 (1:500) antibodies were used to detect primary antibodies for 1hr at room temperature. DNA was stained with Hoechst (Invitrogen). For chromosome spreads, slides were mounted with Vectashield® (Vector Labs). For MI and MII *in situ*, oocytes were passed

through 4 sequentially increasing concentrations of Vectashield® (Vector Labs) in PBS supplemented with 1:250 dilution of Hoechst (Life Technologies) before being mounted in Vectashield® (Vector Labs) using Grace Bio-Labs SecureSealTM imaging spacer (Sigma-Aldrich) to preserve 3D integrity.

Image acquisition

Metaphase I spreads and *in situ* stained Metaphase I and Metaphase II eggs were imaged on a Zeiss LSM780 confocal microscope equipped with 63x/1.4 plan-Apochromat Oil DIC objective lens. Most Metaphase II chromosome spreads were imaged using an Axio Imager Z2 wide-field fluorescent microscope (Zeiss), using 40x/1.3 EC plan-neofluar Oil or 100x/1.3 plan-neofluar Oil and bandpass fluorescent filters appropriate for the fluorophores. All Metaphase I Rec8 *in situ* stainings were collected using the same exposure settings.

Paraffin sectioning and imaging

Tissues were fixed in 10% formalin (VWR), washed in PBS, embedded in paraffin and sectioned at 4 μm sections on a microtome. Following deparaffinisation and rehydration, they were stained for hematoxylin and eosin (H&E). Image acquisition was performed with Panoramic Viewer software.

TEV protease cleavage assay

Rec8$^{TEV/TEV}$ *Wapl*$^{\Delta/\Delta}$ GV oocytes were isolated from 2- to 2.5-month-old *Rec8*$^{TEV/TEV}$*Wapl*$^{fl/fl}$ *(Tg)Zp3*-Cre females in the presence of 0.2 mM IBMX and microinjected using a Pneumatic PicoPump (World Precision Instruments) with 2.3 pmol TEV protease and 2 pmol securin-EGFP mRNA dissolved in RNase-free water (Ambion). After microinjection, oocytes were cultured for 12 hours in M16 supplemented with 0.2 mM IBMX in 5% CO_2 at 37°C.

snHi-C sample acquisition

Mature GV oocytes were isolated from 2- to 2.5- month-old or 14- to 18- month-old C57BL/6J females and 2- to 2.5- month-old or 15-month-old C57BL/Icrf^{at} aged virgin and aged mated female mice. Those oocytes were then further processed using the previously published protocol.[91] After fixation in formaldehyde (2%, Sigma F8775) for 15 min, oocytes were stained with Hoechst (33342, Thermo Fisher Scientific, 0.2μg/ml) to determine the chromatin configuration. For the experiments only oocytes in surrounded-nucleolus stage (SN) were used. Oocytes were then lysed in lysis buffer (10 mM Tris-HCl pH 8.0, 10 mM NaCl, 0.5% (v/v) NP-40 substitute (Sigma), 1% (v/v) Triton X-100 (Sigma), 1 × HaltTM Protease Inhibitor Cocktail (Thermo Scientific)) for at least 15 min on ice, followed by SDS treatment (0.6% SDS in NEB 3 buffer) for 2 hours at 37°C and overnight DpnII (5U, NEB) digestion at 37°C. The nuclei were then ligated (T4 DNA ligase, Thermo Scientific) for 4.5 hours at 16°C, followed by 30 min ligation at room temperature. The DNA was then amplified using illustra GenomiPhi v2 DNA amplification kit (GE Healthcare) with decrosslinking of nuclei at 65°C overnight in sample buffer. High molecular weight DNA was purified using AMPure XP beads (Beckman Coulter), after sonication to obtain fragments of ~300-1300 bp. Libraries were prepared using the NEB Next Ultra Library Prep kit (Illumina) and sequenced on the HiSeq 2500 v4 with 125 bp paired end reads (at VBCF NGS Unit; between 10 and 17 cells per lane) or using the NextSeq high-output kit with 75 bp paired-end reads (at NGS facility in the Department of Totipotency, MPIB; between 12 and 16 samples per kit).

QUANTIFICATION AND STATISTICAL ANALYSIS

Image analysis and quantification

Images were analyzed using Fiji and/or Imaris software. To quantify Rec8 cohesin intensities from chromosome spreads, single z stack files were collapsed with 'Sum of the slices' function of the Fiji software. Mean gray values for cohesin, after background subtraction, was calculated per chromosome spread using Hoechst staining to define the spread area. To quantify Rec8 cohesin intensities from *in situ* Metaphase I oocytes, the Imaris software was used to create a surface mask for DNA. Mean intensity values for chromosomally or centromerically bound Rec8 cohesin were background subtracted (Figures 4B and 4C). To pool the three metaphase I *in situ* experiments, each data point was normalized to its background and the values from both experiments were pooled (Figures 4B and 4C).

Live-cell imaging and Metaphase II chromosome spread analysis was performed using maximum z-projections. *In situ* Metaphase II eggs were analyzed by manually going through acquired z stacks (70-120 slices) in combination with their 3D reconstruction using Fiji or Imaris software. Individual kinetochores signals were analyzed in combination with DAPI staining (DNA) to determine whether each kinetochore is associated with a single chromatid or sister chromatids (dyads). All aneuploidy analysis was performed independently by two or more persons, including at least one blind-scoring person to avoid biases. Chromosomal abnormalities include: 1) Meiosis II PSCC: MII eggs where at least one pair of separated sister centromeres is present, and 2) Chromosomal aneuploidy: Metaphase II eggs where less than or more than 40 sister kinetochores are present. No oocytes were counted twice in any graphs. For example, an oocyte with 39 chromatids is counted once in the chromosomal aneuploidy graph, once in the PSCC graph and once in the chromosomal abnormalities graph. However the oocyte with 39 kinetochores will appear once in the PSCC graph and once in the chromosomal abnormalities graph. A 42 intact kinetochore egg would appear once in the chromosomal aneuploidy graph and once in the chromosomal abnormalities graph. The ratio of hypoploidy to hyperploidy was approximately 1:1 in all cases.

Statistical analysis

Statistical tests and parameters are reported in figure legends. N number in figure legends represents the total number of cells included in each condition. GraphPad Prism version 7.00 for Mac OS X, Microsoft Excel and R studio were used for statistical analysis. A Student's t test was used for analyzing background corrected mean Rec8 fluorescence intensities from chromosome spreads and a two-tailed Mann Whitney U for analysis mean background corrected Rec8 intensities from *in situ* immunofluorescence (D'Agostino normality test for Gaussian distribution). Proportions were compared using the two-sided χ^2 test (Fisher's exact; GraphPad). We note that it is challenging to reach statistical significance for small sample sizes of aged oocytes. It is therefore not a standard in the field to provide measures of statistical significance or standard deviations (for example other studies were aged oocytes were used).[29,80] We nevertheless provide statistics using two-sided Fisher's exact test for the live cell imaging experiments.

For all ploidy data that were not generated from live cell imaging, a 'weight' was calculated for each experiment which reflected the number of cells used in the specific experiment compared to the total number of cells in the experimental condition. The incidence of ploidy was calculated with respect to each experimental weight providing the weighted mean and weighted standard deviations (Microsoft Excel). The package ''weights'' was used in R studio to statistically analyze the weighted means by using a weighted paired Welch Student's t test. Graphs depicting weighted data depict each experiment as a dot and the weighted mean as a cube (with weighted standard deviations). The size of each dot reflects the number of cells used in the respective experiment. The range of cell number that different dot sizes represent, is depicted at the side of each graph.

snHi-C data analysis

snHi-C data were processed as previously published[91] and information about how the samples were pooled is given in Table S1 file (Supplementary Information). Reads were mapped to the mm9 genome using *bwa* and then filtered using *cooltools*. These data were then converted into *cooler* files with heatmaps available at different resolutions.

We analyzed loops by summing up snHi-C contact frequencies for loop coordinates of over 12,000 loops are previously described.[43] By averaging 20 × 20 matrices surrounding the loops and dividing the final result by similarly averaged control matrices, we removed the effects of distance dependence. For display and visual consistency with the loop strength quantification, we set the background levels of interaction to 1; the background is defined as the upper left 6 × 6 and lower right submatrices. For the quantification of loop strength, we divided the average signal in the middle 6 × 6 submatrix by the average signal in top-left and bottom-right (at the same distance from the main diagonal) 6 × 6 submatrices.

Contact probability (Pc(s)) curves were computed from 10-kb binned snHi-C data. We divided the linear genomic separations into logarithmic bins with a factor of 1.3. Data within these log-spaced bins (at distance, s) were averaged to produce the value of Pc(s). Both Pc(s) curves and their log-space slopes are shown following a Gaussian smoothing (using the scipy.ndimage.filters.gaussian_smoothing1d function with radius 0.8). Both the y-axis (i.e., log(Pc(s)) and the x-axis (i.e., log(s)) were smoothed. The average loop strength per condition is determined by bootstrapping 1000 times (for young versus aged and aged virgin versus aged mated oocyte samples while 100 times for +TEV and -TEV injected oocyte samples) over the 12,000 loops as previously described.[43] This is done by random selection of the 12,000 loop coordinates with replacement and using these 1000 (or 100, accordingly) new loop datasets as the basis for the loop strength of the bootstrapped analyses. The average loop size per condition is determined by bootstrapping 100 times over the samples within the condition. This is done by randomly selecting the samples with replacement and creating an aggregate cooler file of those selected samples. Due to the computational intensity of creating cooler files we bootstrapped 100 times unlike the bootstrapping of the loop strength which was done 1000 times for young versus aged and aged virgin versus aged mated oocyte samples while 100 times for +TEV and -TEV injected oocyte samples. In both cases the P value is determined by a Wilcoxon signed-rank test.